A NUMERICAL STUDY OF BAROTROPIC INSTABILITY OF A ZONALLY VARYING JET WITH CYCLIC BOUNDARY CONDITIONS

Bruce Melvin Nagle

NAVAL POSTGRADUATE SCHOOL
Monterey, California

THESIS

A NUMERICAL STUDY OF BAROTROPIC INSTABILITY OF A ZONALLY VARYING JET WITH CYCLIC BOUNDARY CONDITIONS

by

Bruce Melvin Nagle

September 1978

Thesis Advisor: R. T. Williams

Approved for public release; distribution unlimited.

SECURITY CLASSIFICATION OF THIS PAGE (When Data Entered)

REPORT DOCUMENTATION PAGE

READ INSTRUCTIONS BEFORE COMPLETING FORM

1. REPORT NUMBER	2. GOVT ACCESSION NO.
3. RECIPIENT'S CATALOG NUMBER	
4. TITLE (and Subtitle) A Numerical Study of Barotropic Instability of a Zonally Varying Jet with Cyclic Boundary Conditions	5. TYPE OF REPORT & PERIOD COVERED Master's Thesis; September 1978
	6. PERFORMING ORG. REPORT NUMBER
7. AUTHOR(s) Bruce Melvin Nagle	8. CONTRACT OR GRANT NUMBER(s)
9. PERFORMING ORGANIZATION NAME AND ADDRESS Naval Postgraduate School Monterey, California 93940	10. PROGRAM ELEMENT, PROJECT, TASK AREA & WORK UNIT NUMBERS
11. CONTROLLING OFFICE NAME AND ADDRESS Naval Postgraduate School Monterey, California 93940	12. REPORT DATE September 1978
	13. NUMBER OF PAGES 71
14. MONITORING AGENCY NAME & ADDRESS(if different from Controlling Office) Naval Postgraduate School Monterey, California 93940	15. SECURITY CLASS. (of this report) Unclassified
	15a. DECLASSIFICATION/DOWNGRADING SCHEDULE

16. DISTRIBUTION STATEMENT (of this Report)

Approved for public release; distribution unlimited.

17. DISTRIBUTION STATEMENT (of the abstract entered in Block 20, if different from Report)

18. SUPPLEMENTARY NOTES

19. KEY WORDS (Continue on reverse side if necessary and identify by block number)

20. ABSTRACT (Continue on reverse side if necessary and identify by block number)

Tupaz et al. (1978) formulated a model to study the behavior of waves in an unstable jet which varied downstream. The linearized barotropic vorticity equation was solved numerically. Waves were forced with a fixed period on the eastern boundary and a radiation condition was applied on the western boundary.

DD FORM 1 JAN 73 1473 EDITION OF 1 NOV 65 IS OBSOLETE
S/N 0102-014-6601 |

SECURITY CLASSIFICATION OF THIS PAGE (When Data Entered)

In this thesis, cyclic boundary conditions are used on the eastern and western boundaries. The numerical solutions show amplitude growth in time which is approximately exponential. The solutions are normalized and the wave structure is obtained during three time segments. The wave structures are not the same during these segments, but they are very similar in areas of large amplitudes. In these regions the behavior is very similar to that obtained by Tupaz et al. (1978).

A Numerical Study of Barotropic Instability of a Zonally Varying Jet with Cyclic Boundary Conditions

by

Bruce Melvin Nagle
Captain, United States Air Force
B.S., Mathematics, Westminster College, 1966
B.S., Meteorology, University of Utah, 1968
MBA., Golden Gate University, 1976

Submitted in partial fulfillment of the requirements for the degree of

MASTER OF SCIENCE IN METEOROLOGY

from the

NAVAL POSTGRADUATE SCHOOL
September 1978

ABSTRACT

Tupaz et al. (1978) formulated a model to study the behavior of waves in an unstable jet which varied downstream. The linearized barotropic vorticity equation was solved numerically. Waves were forced with a fixed period on the eastern boundary and a radiation condition was applied on the western boundary.

In this thesis, cyclic boundary conditions are used on the eastern and western boundaries. The numerical solutions show amplitude growth in time which is approximately exponential. The solutions are normalized and the wave structure is obtained during three time segments. The wave structures are not the same during these segments, but they are very similar in areas of large amplitudes. In these regions the behavior is very similar to that obtained by Tupaz et al. (1978).

TABLE OF CONTENTS

LIST OF FIGURES

ACKNOWLEDGEMENTS

The author expresses his sincerest appreciation to Professor R. T. Williams and CDR J. B. Tupaz for their guidance throughout this research.

Many thanks are also extended to Dr. T. Rosmond for his help in applying subroutine POISS to the numerical model, and C.-P. Chang for reading the thesis and making helpful comments.

A very special appreciation is extended to Manus Anderson, Edwin Donnellan and Joanne Kallweit of the W. R. Church Computer Center who provided outstanding computer support.

This work was supported by the Atmospheric Research Section, National Science Foundation, under Grant ATM 77-14821, and by the Naval Environmental Prediction Research Facility.

I. INTRODUCTION

A jet, regardless of its latitudinal position in the atmosphere, may contain regions of large vorticity gradients where the necessary condition for barotropic instability is locally satisfied. Synoptic-scale moving disturbances occurring at the level of a moderately strong easterly jet south of the Tibetan high near 200 mb level appear to arise from barotropic instability of the mean flow (Krishnamurti, 1971a, 1971b). If the observed disturbances are the result of barotropic instability, they will extract energy from the mean flow.

Many investigators have studied the linear stability of barotropic zonal flows over the years. Krishnamurti's observational and Colton's (1973) numerical studies both showed that the zonal variation of the jet apparently had significant effects on the dynamic behavior of the transient disturbances.

Tupaz et al. (1978) further extended the study of the zonal variation of the basic flow. A numerical model was developed based on the linearized non-divergent barotropic vorticity equation on a beta-plane. This study examined the dynamics of transient barotropic waves in a region of variable mean wind. The mean zonal wind was an easterly hyperbolic secant-squared, or Bickley, jet and the mean meridional wind was derived so that the mean flow would be non-divergent. Using the numerical model, a periodic forcing was applied on the inflow (eastern) boundary to generate waves which were

allowed to propagate through the channel and out through the western boundary. As the waves moved, they reacted to the local stability properties of the mean flow, whereas at each point the fields varied periodically. The results, which were obtained from long term integration, were compared with the parallel flow theory by constructing a simple mechanistic analytical model which incorporated the local stability concept of the parallel flow theory.

In this thesis, the model developed by Tupaz et al. (1978) is modified by changing the boundary conditions. The quantities on the eastern and western ends of the channel are set equal to enforce cyclic continuity. This allows a wider variety of wind profiles to be considered as long as they are periodic in x. The use of these boundary conditions will also improve our understanding of the mathematical behavior of waves in a mean flow with downstream variation.

II. BASIC EQUATIONS

A. GENERAL FORMULATION

This study employs the barotropic vorticity equation to describe motion in a periodic channel. The development which follows Tupaz et al. (1978) begins with the barotropic vorticity equation on a beta (β) plane:

$$\frac{\partial \zeta}{\partial t} + u \frac{\partial \zeta}{\partial x} + v \frac{\partial \zeta}{\partial y} + \beta v = Q - D_f \zeta \ , \qquad (2.1)$$

where

$$\zeta \equiv \frac{\partial v}{\partial x} - \frac{\partial u}{\partial y} \ . \qquad (2.2)$$

Here, β is the constant value of the north-south gradient of Coriolis parameter computed at 10^{o} latitude. Q is a forcing function which represents the non-barotropic and diabatic effects which are required to maintain the basic state vorticity field, and D_f is a frictional coefficient. The motion is assumed to be non-divergent so that a stream function (ψ) can be introduced which is defined by

$$u = - \frac{\partial \psi}{\partial y} \ , \qquad v = \frac{\partial \psi}{\partial x} \ . \qquad (2.3)$$

The vorticity becomes

$$\zeta = \nabla^2 \psi \ . \qquad (2.4)$$

The non-divergent barotropic vorticity equation may now be written,

$$\frac{\partial}{\partial t}\nabla^2\psi - \frac{\partial\psi}{\partial y}\frac{\partial\nabla^2\psi}{\partial x} + \frac{\partial\psi}{\partial x}\frac{\partial\nabla^2\psi}{\partial y} + \beta\frac{\partial\psi}{\partial x} = Q - D_f\nabla^2\psi \ . \qquad (2.5)$$

The linearization of eq. (2.5) is accomplished by separating the stream function into its mean (bar) and perturbation (prime) quantities of the form:

$$\psi(x,y,t) = \bar{\psi}(x,y) + \psi'(x,y,t) \ , \qquad (2.6)$$

where $|\psi'| << |\bar{\psi}|$. Substituting (2.6) into (2.5) and dropping the quadratic terms in ψ' leads to

$$\frac{\partial}{\partial t}\nabla^2\psi' - \frac{\partial\bar{\psi}}{\partial y}\frac{\partial}{\partial x}\nabla^2\psi' + \frac{\partial\bar{\psi}}{\partial x}\frac{\partial}{\partial y}\nabla^2\psi' - \frac{\partial\psi'}{\partial y}\frac{\partial}{\partial x}\nabla^2\bar{\psi}$$

$$+ \frac{\partial\psi'}{\partial x}\frac{\partial}{\partial y}\nabla^2\bar{\psi} + \beta\frac{\partial\psi'}{\partial x} = - D_f\nabla^2\psi' \qquad (2.7)$$

It is assumed that $Q' = 0$ and $\bar{Q}$ is defined in such a way that $\bar{\psi}$ is a steady-state solution of (2.5). Equation (2.7) can also be rewritten in Jacobian form such that

$$\nabla^2\frac{\partial\psi'}{\partial t} = - \bar{J}(\bar{\psi},\nabla^2\psi') - \bar{J}(\psi',\nabla^2\bar{\psi}) - \beta\frac{\partial\psi'}{\partial x}$$

$$- D_f\nabla^2\psi' \ , \qquad (2.8)$$

where $J(a,b) = \frac{\partial a}{\partial x}\frac{\partial b}{\partial y} - \frac{\partial a}{\partial y}\frac{\partial b}{\partial x}$.

Equation (2.8) is a Poisson equation for the tendency of the perturbation stream function ($\frac{\partial\psi'}{\partial t}$).

Equation (2.7) is solved in a channel defined by

$$-D \leq y \leq D$$

$$x_W \leq x \leq x_E \ .$$

The boundary conditions of the north-south walls $y = \pm D$ are

$$\psi' = 0 \ . \tag{2.9}$$

Cyclic boundary conditions are used in the east-west direction. Tupaz et al. (1978) applied a time-periodic forcing on the eastern boundary to introduce waves into the region from the east, and used a radiation condition for both tendency and vorticity at the western boundary to allow the waves to move smoothly through the boundary.

B. ZONALLY VARYING BASIC FLOW

The basic velocity field is defined by an easterly Bickley jet

$$\bar{u}(x,y) = U(x)\ \mathrm{sech}^2\left(\frac{y}{d(x)}\right) - U_o = -\frac{\partial \bar{\psi}}{\partial y} \ . \tag{2.10}$$

Here, $d(x)$ is a characteristic length scale of the jet, $U(x)$ is the maximum velocity at $y = 0$, and U_o is a constant velocity. The basic flow stream function is specified to be constant at the northern and southern boundaries ($y = \pm D$). Equation (2.10) can be integrated to give

$$\bar{\psi}(x,y) = U(x)\ d(x)\left\{\tanh\left(\frac{y}{d(x)}\right) + \tanh\left(\frac{D}{d(x)}\right)\right\} - U_o(y+D) + \bar{\psi}(-D) \ , \tag{2.11}$$

where

$$U(x) = \frac{\bar{\psi}(D) + 2U_o D - \bar{\psi}(-D)}{2d(x)} \coth\left(\frac{D}{d(x)}\right) . \quad (2.12)$$

Therefore, if $d(x)$ varies slowly in x, so does the basic flow. The x-variation for the characteristic length scale is given by

$$d = \frac{850 \text{ km} + 350 \text{ km}\{\cos[2\pi \frac{(x-\tilde{x}_o)}{\tilde{L}}]\}}{1200 \text{ km}} ,$$

$$-\tilde{x}_o \leq x \leq \tilde{x}_o ,$$

$$x \leq -\tilde{x}_o , \quad (2.13)$$

$$x \geq \tilde{x}_o .$$

Here, $\tilde{x}_o$ is the longitude where the x-variation of the cosine function starts and $\tilde{L}$ is the wavelength of this variation.

III. FINITE DIFFERENCE EQUATIONS

Equation (2.7) is solved by finite differences. Centered time differences are used except for the friction term which is approximated with a forward step. The Jacobians are computed with the form which was developed by Arakawa (1966) for non-linear conservation.

The tendency of the disturbance stream function is defined by

$$T^{t}_{i,j} \equiv \left[\frac{\partial \psi'}{\partial t}\right]^{t}_{i,j} , \qquad (3.1)$$

where superscript t is the current time and subscripts i and j refer to the x and y grid points, respectively. In the following finite difference equations, Δt(1 hour) is the time step. Δx(375 km) and Δy(125 km) are the x and y grid point intervals, respectively. Equation (2.7) is written using the Leapfrog finite difference scheme:

$$\nabla^2 T^{t}_{i,j} = -\mathcal{J}^{t}_{i,j}[\bar{\psi},\nabla^2\psi'] - \mathcal{J}^{t}_{i,j}[\psi',\nabla^2\bar{\psi}]$$

$$- \beta \frac{[\psi^{t}_{i+1,j} - \psi^{t}_{i-1,j}]}{2\Delta x} - D_f \nabla^2 \psi'^{\,t-\Delta t}_{i,j} , \qquad (3.2)$$

$$\psi'^{\,t+\Delta t}_{i,j} = \psi'^{\,t-\Delta t}_{i,j} + T_{i,j}\Delta t . \qquad (3.3)$$

The finite difference form for the Laplacian of the tendency is given by

$$\nabla^2 T^t_{i,j} \equiv \frac{T^t_{i+1,j} - 2T^t_{i,j} + T_{i-1,j}}{\Delta x^2} + \frac{T^t_{i,j+1} - 2T_{i,j} + T_{i,j-1}}{\Delta y^2} \tag{3.4}$$

and for the Jacobian terms it is given by:

$$\overset{①}{J}{}^t_{i,j} = \frac{1}{4\Delta x \Delta y}[(\bar{\psi}_{i+1,j} - \bar{\psi}_{i-1,j})(\zeta'^t_{i,j+1} - \zeta^t_{i,j-1}) \tag{3.5}$$

$$- (\bar{\psi}_{i,j+1} - \bar{\psi}_{i,j-1})(\zeta'^t_{i+1,j} - \zeta'^t_{i-1,j})] \ ,$$

$$\overset{②}{J}{}^t_{i,j} = \frac{1}{4\Delta x \Delta y}[\bar{\psi}_{i+1,j}(\zeta'^t_{i+1,j+1} - \zeta'^t_{i+1,j-1}) \tag{3.6}$$

$$- \bar{\psi}_{i-1,j}(\zeta'^t_{i-1,j+1} - \zeta'^t_{i-1,j-1})$$

$$- \bar{\psi}_{i,j+1}(\zeta'^t_{i+1,j+1} - \zeta'^t_{i-1,j+1})$$

$$+ \bar{\psi}_{i,j-1}(\zeta'^t_{i+1,j-1} - \zeta'^t_{i-1,j-1})] \ ,$$

and

$$\overset{③}{J}{}^t_{i,j} = \frac{1}{4\Delta x \Delta y}[\zeta'^t_{i,j+1}(\bar{\psi}_{i+1,j+1} - \bar{\psi}_{i-1,j+1}) \tag{3.7}$$

$$- \zeta'^t_{i,j-1}(\bar{\psi}_{i+1,j-1} - \bar{\psi}_{i-1,j-1})$$

$$- \zeta'^t_{i+1,j}(\bar{\psi}_{i+1,j+1} - \bar{\psi}_{i+1,j-1})$$

$$+ \zeta'^t_{i-1,j}(\bar{\psi}_{i-1,j+1} - \bar{\psi}_{i-1,j-1})] \ ,$$

where

$$\mathcal{J}^{t}_{i,j}[\bar{\psi},\nabla^2\psi'] = \frac{\overset{①}{\mathcal{J}}{}^{t}_{i,j} + \overset{②}{\mathcal{J}}{}^{t}_{i,j} + \overset{③}{\mathcal{J}}{}^{t}_{i,j}}{3} . \qquad (3.8)$$

$\mathcal{J}^{t}_{i,j}[\psi',\nabla^2\bar{\psi}]$ is expanded in the same manner as for (3.8). This Jacobian conserves both kinetic energy and enstrophy in the non-linear formulations (Arakawa, 1966).

A forward time step is used for the initial time step and every 30 time steps thereafter to damp the internal gravity waves produced by the leapfrog method. A Matsuno finite difference scheme is tested in place of the forward time step and the results show that the Matsuno scheme provides further damping, but that the change is not significant.

The boundary conditions employed by Tupaz et al. (1978) relieved the problem of reflection of incident waves from the boundary back into the interior region (Pearson, 1974). An Euler-backward finite difference scheme was employed every time step to provide additional damping of the short waves.

The frictional terms are evaluated at the previous time step in order to insure linear computation stability (Haltiner, 1971).

The Poisson Eq. (3.1) is solved for the tendency using the POISS subroutine which is a cyclic reduction algorithm for solving block tridiagonal systems of arbitrary dimensions with Dirichlet boundary conditions (Swarztrauber and Sweet, 1978).

The subroutine POISS solves the linear system of equations of the form:

$$A_i X_{i-1,j} + B_i X_{i,j} + C_i X_{i+1,j} + X_{i,j-1} - 2X_{i,j} + X_{i,j+1} = Y_{i,j}$$

$$\text{for } I = 1,2, \ldots M \text{ and } J = 1,2, \ldots N . \tag{3.9}$$

The east-west boundary conditions for all quantities are represented by

$$X_{i,o} = X_{i,I} \qquad i = 0, I$$

$$X_{i,J+1} = X_{i,1} \qquad j = 0, J+1 \tag{3.10}$$

It should be noted that Eq. (3.9) is not in the correct form which satisfies the model. Therefore, the model must be flipped prior to entering the solver and then flipped back upon exiting with the solved eigenvalue-solutions.

IV. LOCAL STABILITY OF BASIC FLOW

A parallel flow model of Williams et al. (1971) is used to determine the local growth rate of the variable mean flow. This is taken from Tupaz et al. (1978) and then transposed to fit the basic flow model used for this study in order to gain some insight on the stability characteristics of the mean flow. This model is hereafter referenced as the parallel flow model. If $\partial\bar{\psi}/\partial x$ is set equal to zero in (2.5) the governing equation of this model is

$$\left[\frac{\partial}{\partial t} + \bar{u}\,\frac{\partial}{\partial x} + D_f\right]\nabla^2\psi' + \left[\beta - \frac{\partial^2\bar{u}}{\partial y^2}\right]\frac{\partial\psi'}{\partial x} = 0\,, \qquad (4.1)$$

$$\bar{u}(y) = -U\,\mathrm{sech}^2\left(\frac{y}{d}\right) + U_o$$

where U is a specified constant that scales the magnitude of the central velocity of the Bickley jet ($y=0$). The characteristic length d is also a specified constant. Equation (4.1) is solved with the initial value technique used by Williams et al. (1971). Assuming that all perturbations are periodic in x, Eq. (4.1) is Fourier transformed in x and the resulting equations are integrated until the solution grows with a constant exponential rate. This approach gives the growth rate, phase speed and wave number structure of the most unstable meridional mode as a function of the zonal wave number k.

In general, these equations have a set of normal mode solutions and a continuous spectrum of solutions (Case, 1960; Pedlosky, 1964 and Yanai and Nitta, 1968). However, only the normal mode solutions can give significant growth and the most unstable mode will dominate after a sufficient period of time.

Figure 1 shows the growth rate (n) corresponding to the most unstable wavelengths (L) as a function of x based on the parallel flow model. The parameters for the mean flow are given in Section V. The largest growth rate occurs at x=0 where the jet achieves its maximum central velocity [$\bar{u}$ = - 30 m sec^{-1}]. In the inflow and outflow region for x < - 11,100 km and x > 11,100 km, respectively, the growth rate becomes negative and approaches the linear frictional damping rate. The most unstable wavelengths range from 3650 km at x=0 to 4600 km in the inflow and outflow regions. This variation follows the variation in the y-scale of jet d(x) which is given by (2.16) (Tupaz et al., 1978).

Eigensolutions of the most unstable discrete mode for two jet profiles are shown in Fig. 2. Only the lower half of the y domain is shown because the solutions are symmetric about y=0. Both solutions show barotropic growth as the phase tilt is opposite to the shear in $\bar{u}$. The maximum tilt occurs at x=0 where the growth rate is the largest. In addition, the eigensolution amplitude is a maximum at y= 0 for x=0, but at x = 9314 km the maximum has shifted to y = $\pm$ 800 km.

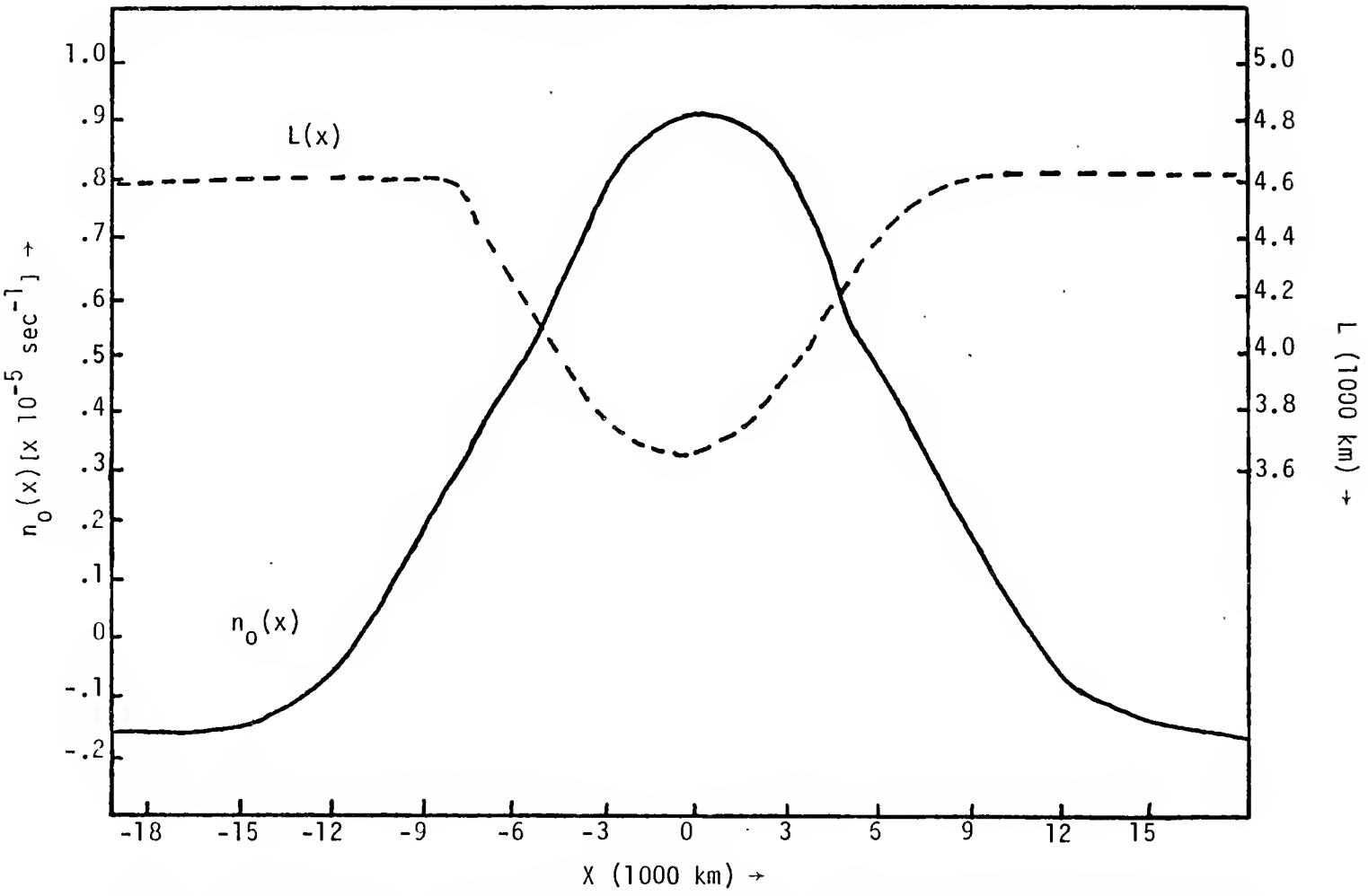

Fig. 1. (a) The most unstable wavelength L(x), and (b) corresponding local growth rate $n_0(x)$, based on the parallel flow model.

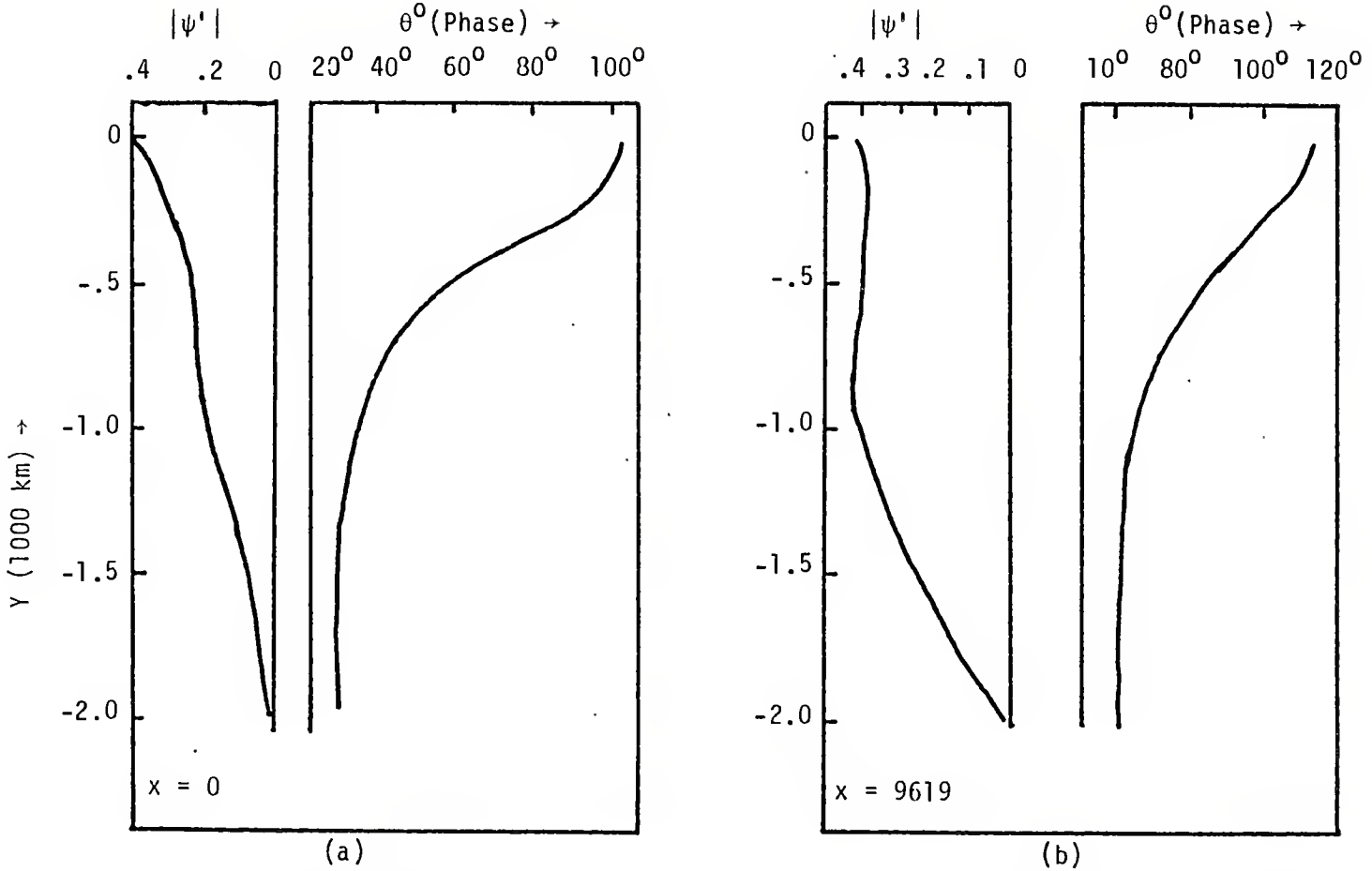

Fig. 2. Parallel flow model wave structure of the most unstable mode for longitudes: (a) x=0 and (b) x = ± 9619.

V. NUMERICAL RESULTS FOR EXPERIMENT I

The numerical investigation of the variable mean wind model comprises two experiments. Experiment I is the principal one and it employs the same friction that was used by Tupaz et al. (1978). A friction coefficient of $D_f = 0.15 \times 10^{-5}$ sec^{-1} is used which is equivalent to an e-folding decay time of approximately 7.7 days. The second experiment is the frictionless case and will be discussed in Section VI.

The following parameters are used in Experiment 1.

$2D = 4000$ km, $x_E - x_W = 40{,}125$ km, $\bar{u}(0,0) = -30$ m s^{-1} ,

$U_o = 0$, $\tilde{L} = 36{,}000$ km, $\Delta x = 375$ km, $\Delta y = 125$ km ,

$\Delta t = 1$ hr, $\tilde{x}_o = \pm 18{,}000$ km

Figures 3 and 4 show the stream function $\bar{\psi}(x,y)$ and the zonal velocity $\bar{u}(x,y)$ which are derived from the above parameters. The model has 108 grid intervals in the x-direction and 32 intervals in the y-direction. Tupaz et al. (1978) used the same domain, but his mean flow was not the same at $x = x_E$ and $x = x_W$. However in this study, the scale of variation of the jet is reduced to insure that the basic zonal velocity would be periodic in the inflow and outflow regions. Equation (2.13) specifies that the jet scale, d(x), varies between 500 km at $\bar{u}(x,0)_{max}$ and 1200 km at $\bar{u}(x,0)_{min}$.

The initial disturbance field is of the form:

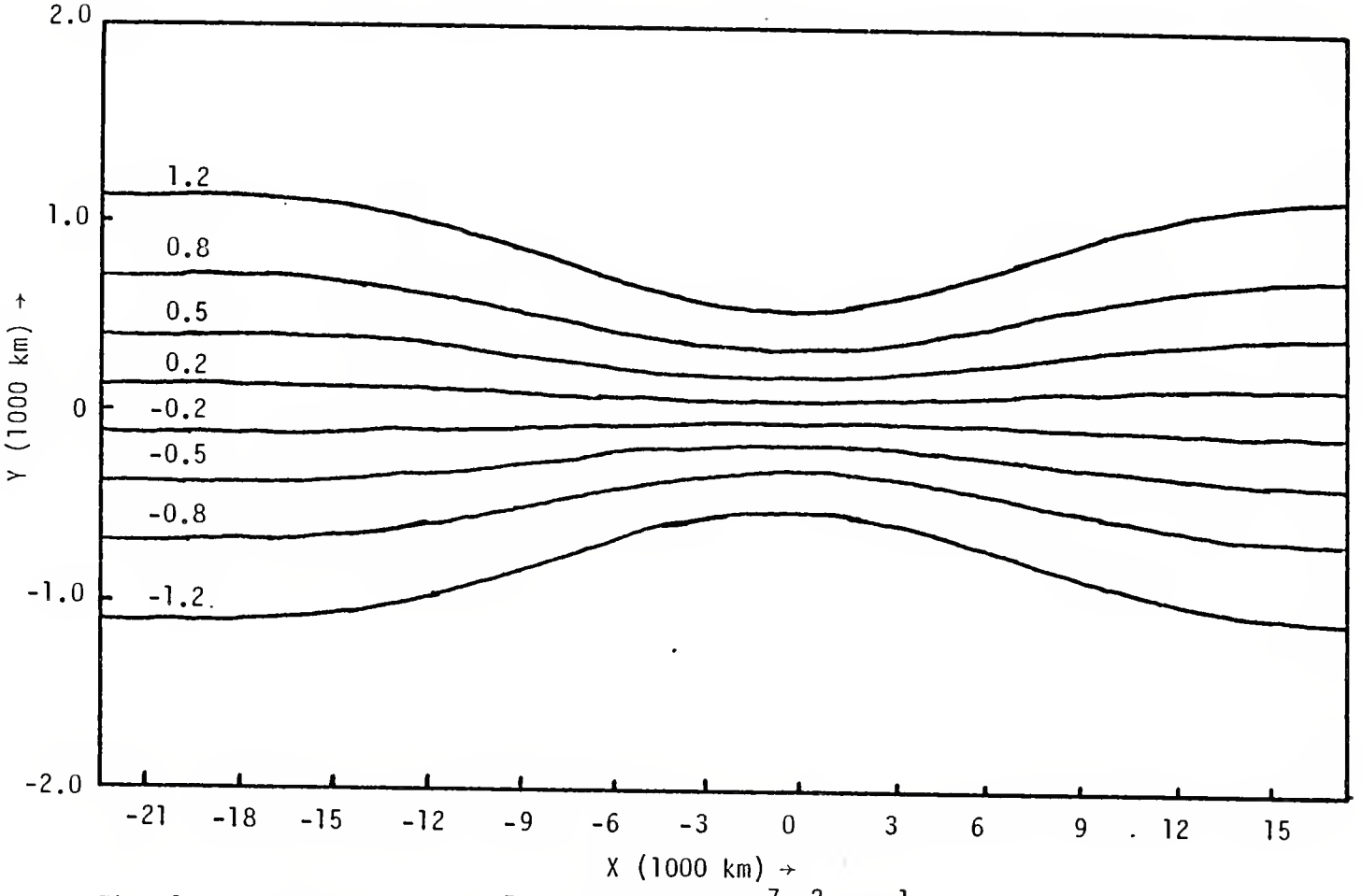

Fig. 3. Experiment I. The $\bar{\psi}(x,y)$ field (x 10^7 m^2 sec^{-1}).

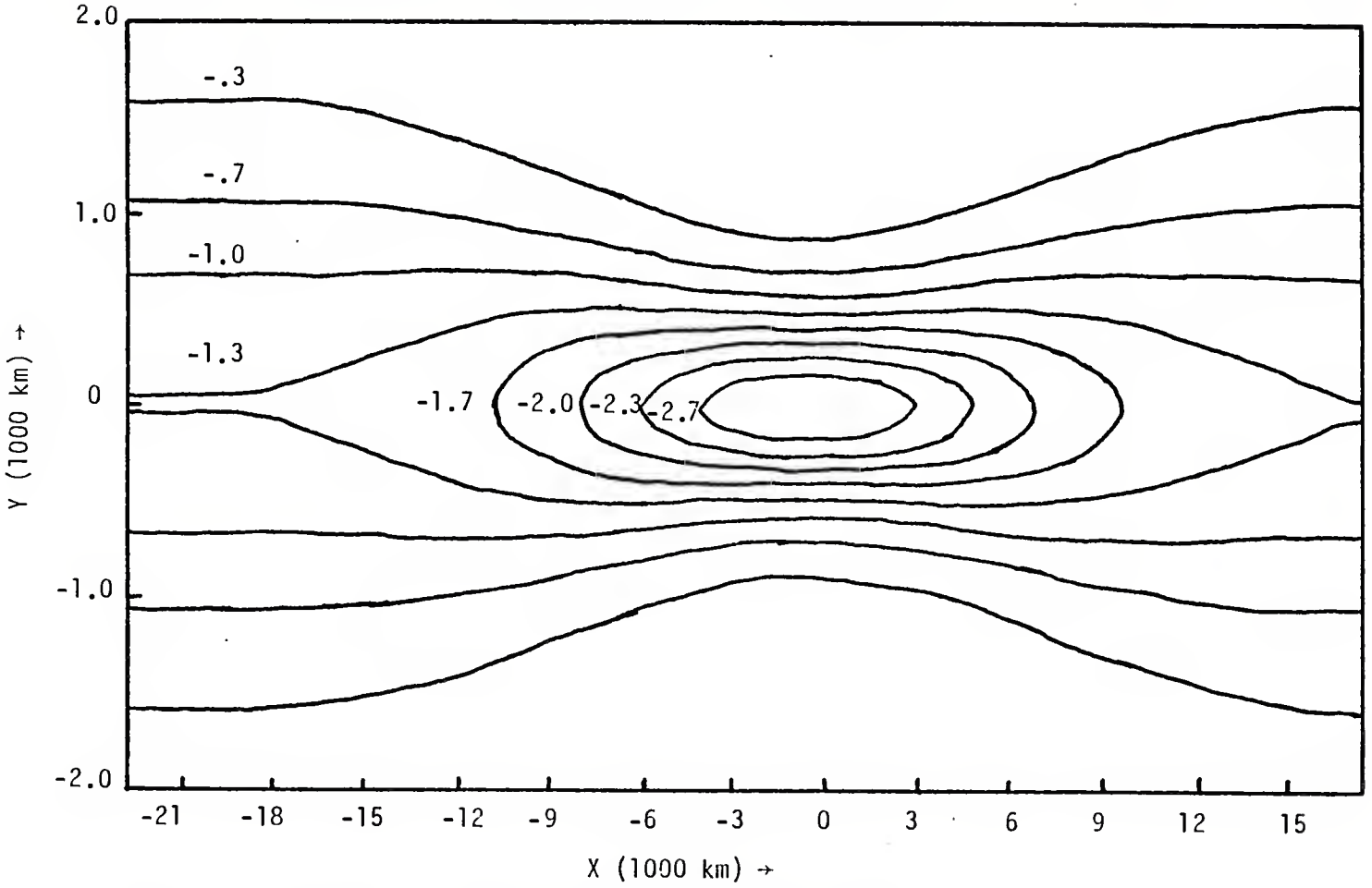

Fig. 4. Experiment I. The $\bar{u}(x,y)$ field (x 10 m sec^{-1}).

$$\psi'(x,y,o) = \sin\frac{\pi y}{2D} \frac{\cos 2\pi\ 10x}{x_E - x_W} . \qquad (5.1)$$

A wave number of 10 is chosen as a result of the average wavelength which was obtained by Tupaz et al. (1978). The initial conditions and the jet flow are both symmetric about $y=0$ and this symmetry is maintained throughout the integration. Therefore, only the lower half of the y plane will be depicted in the results of both experiments.

The integration of the numerical model is extended for a period of 170 days. A close examination of wave structure, phase tilt, period, wavelength, and spatial growth is made for the segments 80-87 days, 125-133 days and 150-157 days. Overall growth occurs during the entire period and is expected since the waves travel through the region and then reappear at the input boundary. It was expected that the overall growth would be exponential in behavior. Figure 5 shows the root mean square for the entire domain of ψ' plotted on a log scale vs time. If the growth were truly exponential, the curve in Fig. 5 would be linear. But in fact the curve is quasi-linear with departures from the linear behavior occurring periodically about every 56 days. Figure 5 shows the first departure occurs near t=21 days and continues for 28 days. It should also be noted that the growth rate is negative from t=38 days to t=47 days. This departure from the linear appears again at t=75 days for 25 days and again at t=135 days for 26 days.

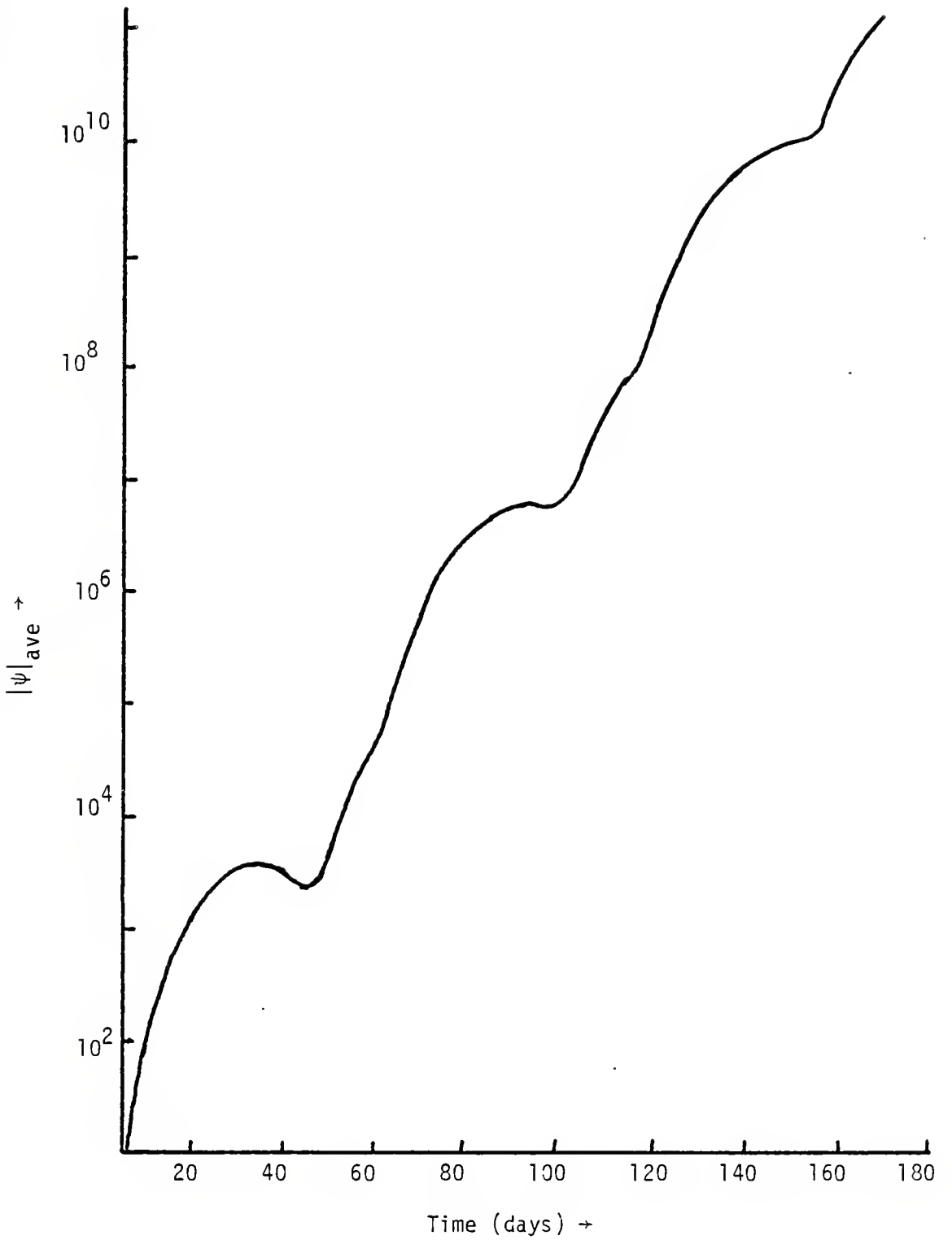

Fig. 5. Experiment I. $|\psi|_{ave}$ as a function of time, where $|\psi|_{ave}$ is the root mean square of ψ'.

The ψ' field at t=30 days is shown in Fig. 6. An entire train of barotropic waves actually exists throughout the length of the channel, but the waves upstream of x = -3500 km and in the outflow region are not shown because of their relatively small amplitude. This is the same type of wave behavior observed by Tupaz et al. (1978).

The phase is calculated for the segments mentioned earlier. This is accomplished by observing each grid point in the ψ' field and recording the first three times it passes through zero in either direction. A seven day period (P) is used in order to insure that a full period is recorded. Tupaz et al. (1978) observed a periodicity of 3.25 days. The actual phase for each grid point is computed using the following formula:

$$\theta = \frac{360^{o}(N-N_{o})}{P} \qquad (5.2)$$

where N represents the first time it passed through zero and N_o is the starting point in time of the sign calculations for each time segment. Although the wave continues to grow during the time segment, the period should not change appreciably. Figure 7 represents an analyzed section of the phase tilt for the segment 80-87 days. We note that all the waves shown tilt oppositely to the mean wind shear, which is necessary for barotropic instability. The maximum tilt is observed downstream of x=0 where the jet velocity is maximum.

The periods at y=0 and y = $\pm$ 750 km for all three time segments are shown in Figs. 8-10. Although the periodicity is

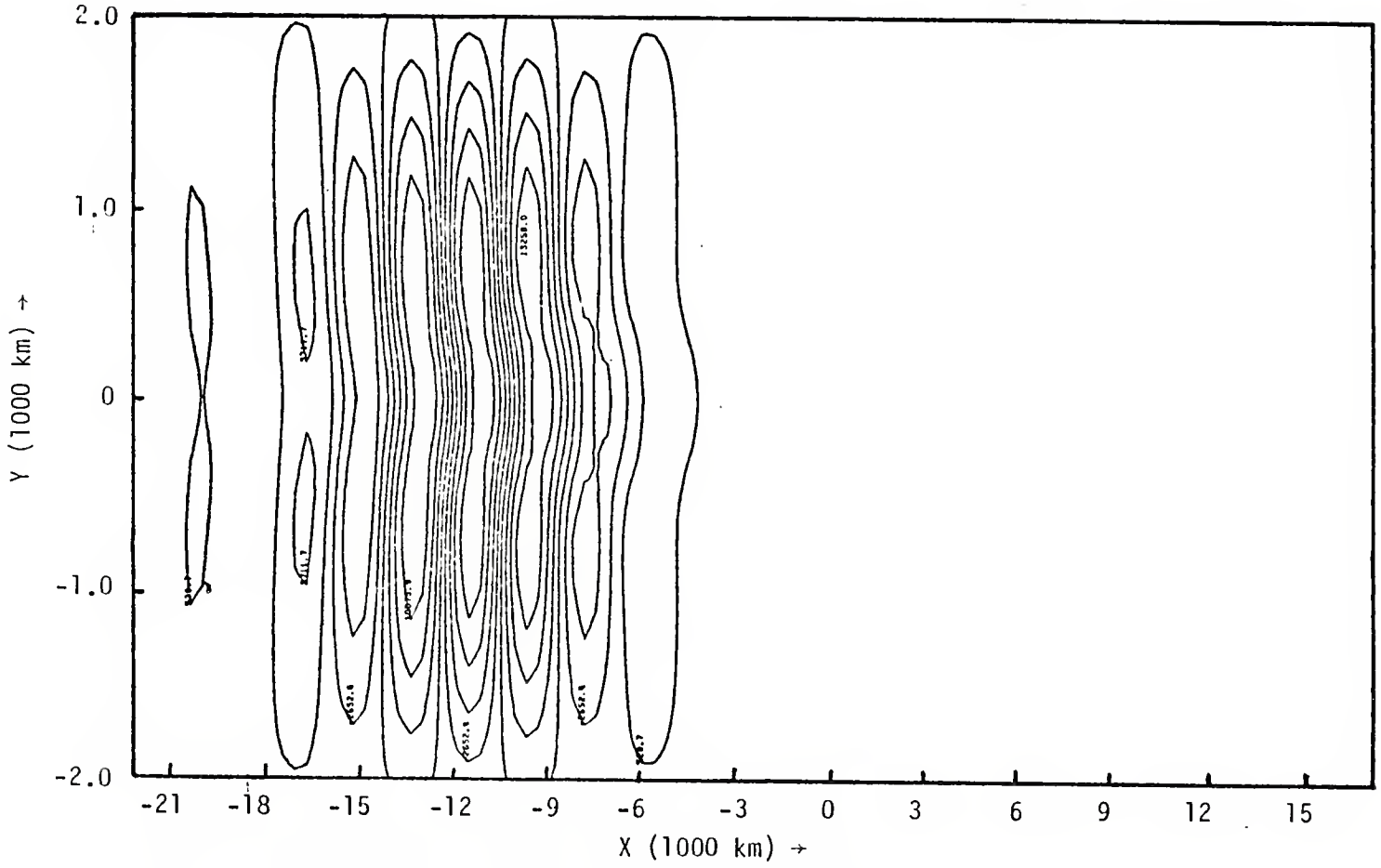

Fig. 6. Experiment I. The ψ' field at t = 30 days.

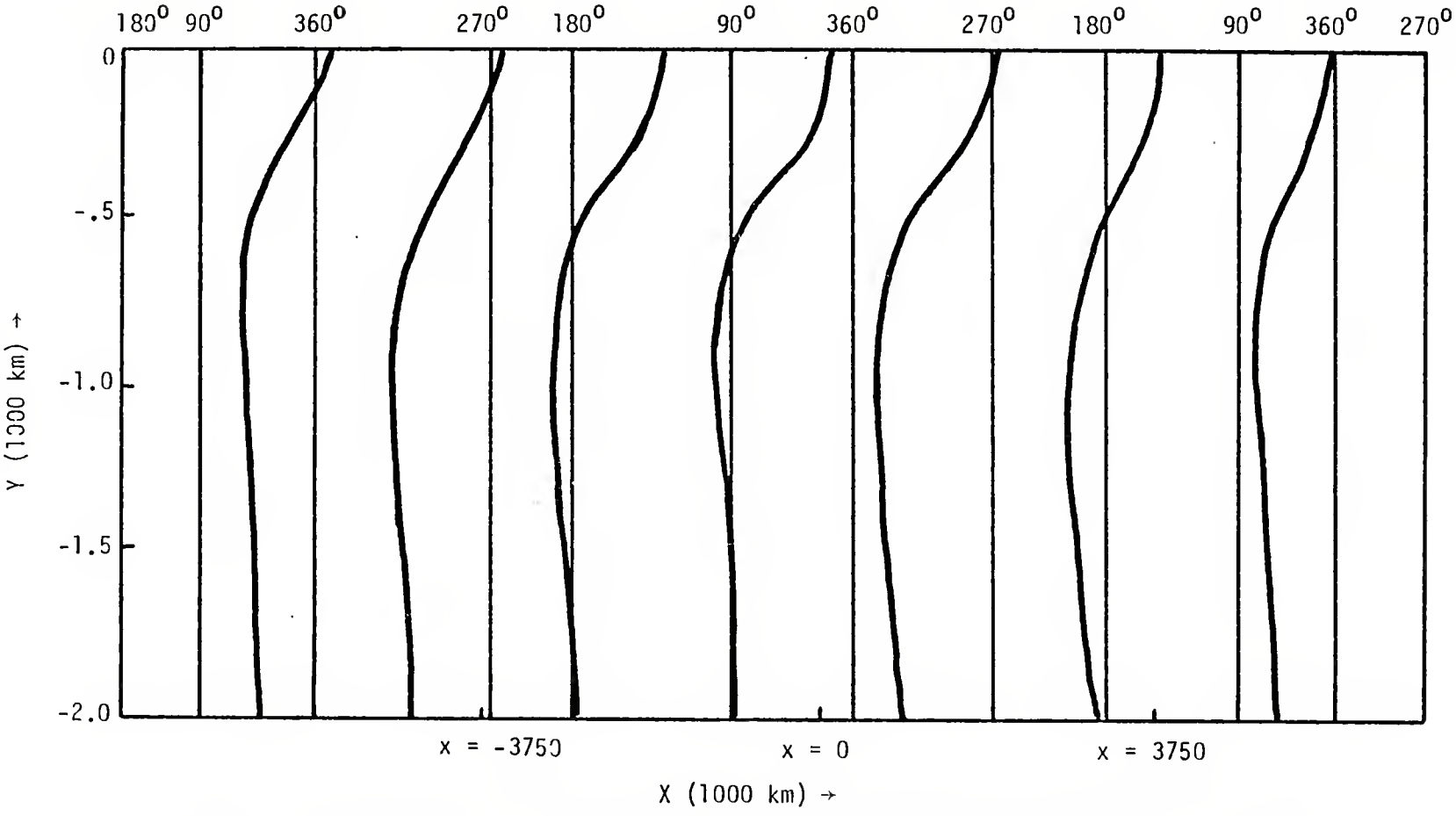

Fig. 7. Experiment I. Analyzed section of phase θ during the segment 80-87 days.

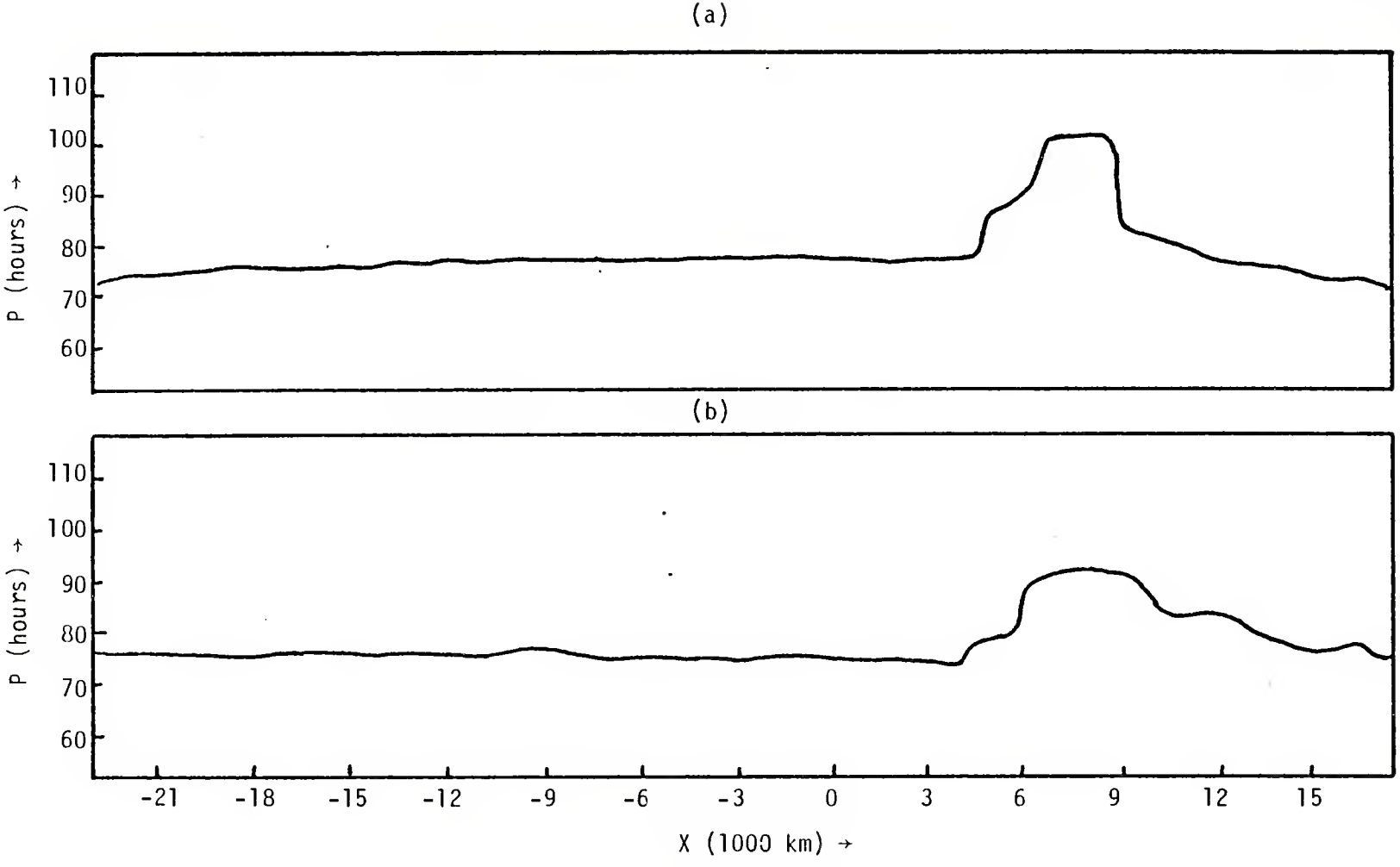

Fig. 8. Experiment I. Periods of the numerical model for the time segment 80-87 days for latitudes: (a) y = 0 and (b) y = $\pm$ 750 km.

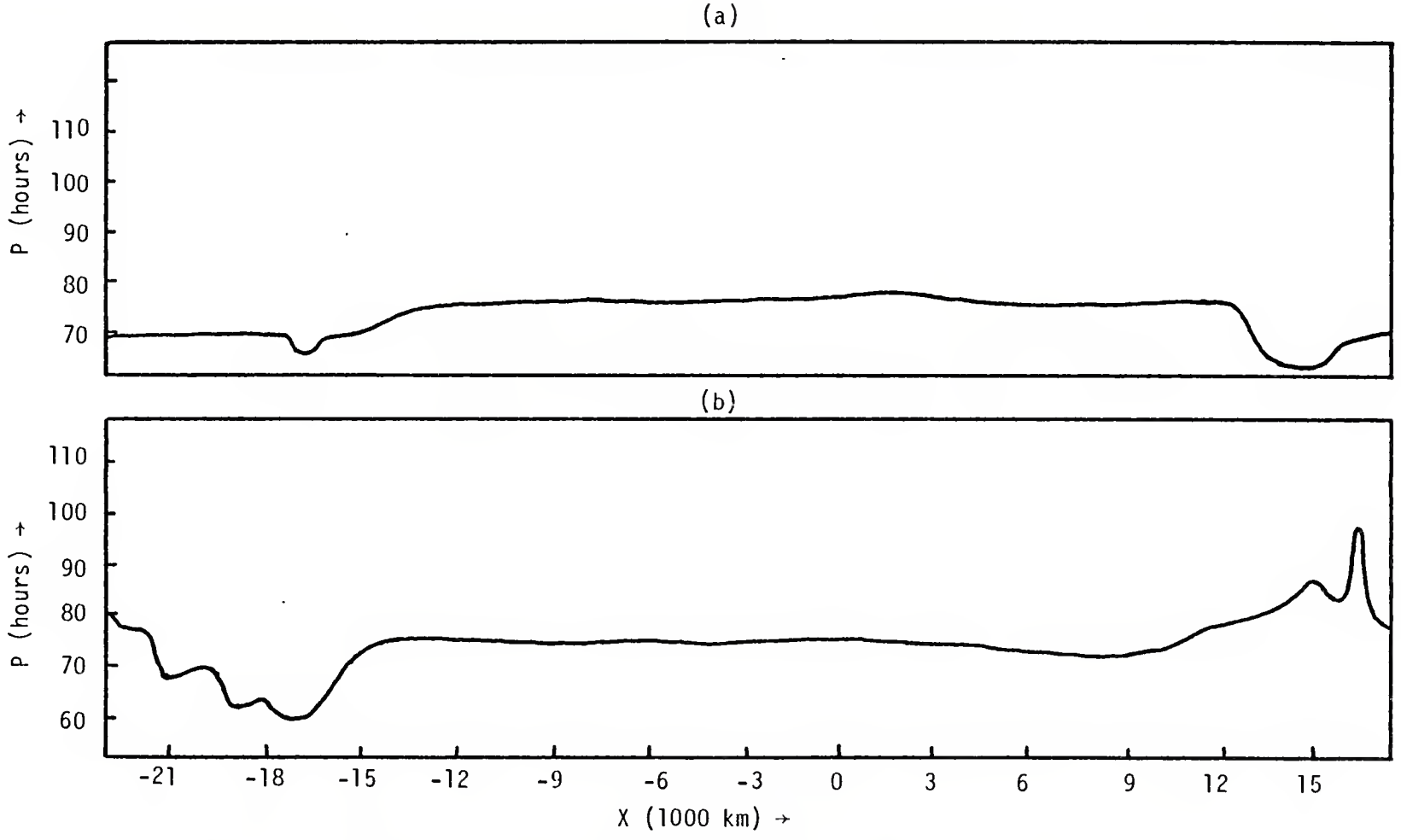

Fig. 9. Experiment I. Periods of the numerical model for the time segment 125-133 days for latitudes: (a) $y = 0$ and (b) $y = \pm 750$ km.

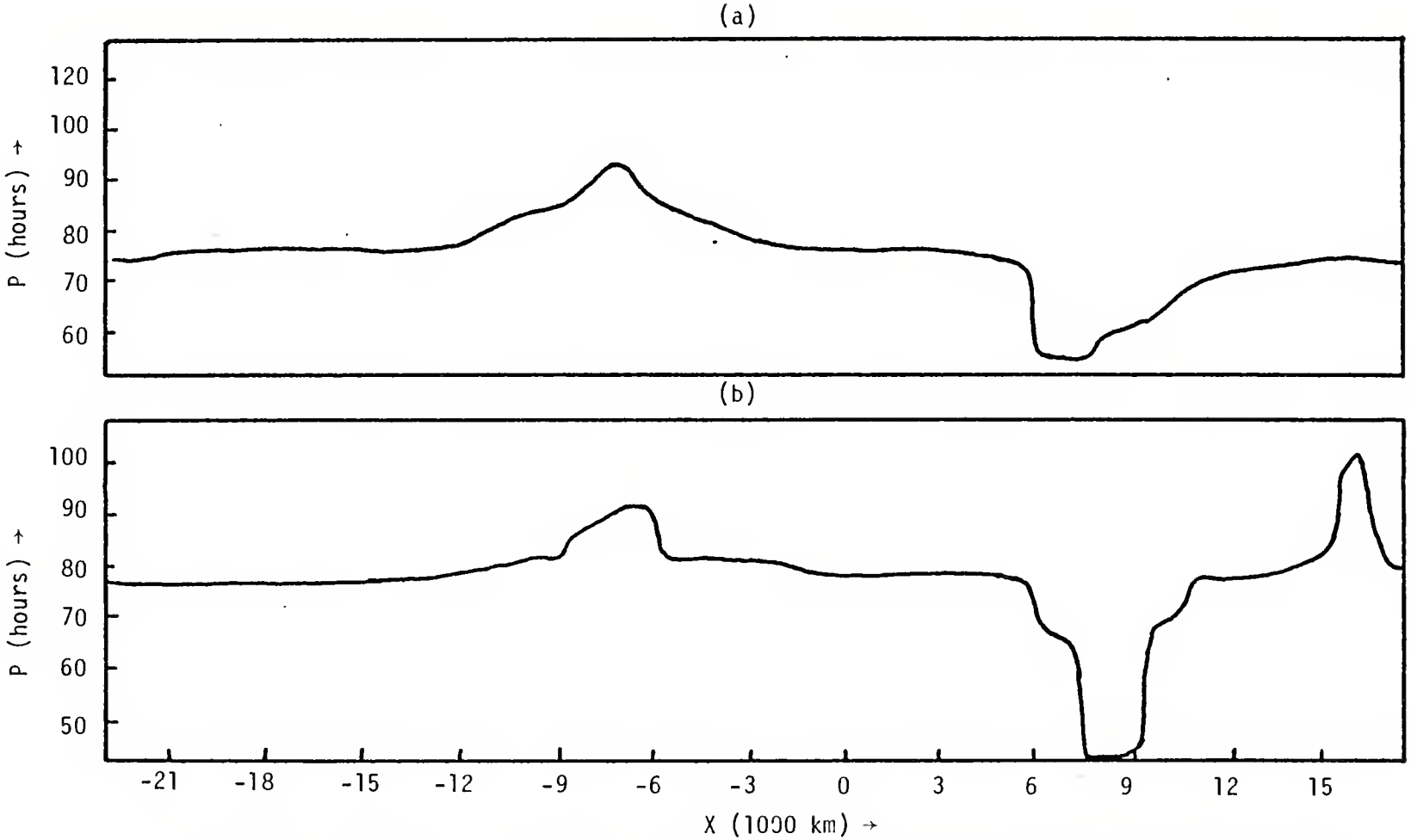

Fig. 10. Experiment I. Periods of the numerical model for the time segment 150-157 days for latitudes: (a) $y = 0$ and (b) $y = \pm 750$ km.

not constant, it is about 77 hours (3.2 days). This is also representative of the entire channel. Deviations near the inflow/outflow boundaries could be attributed to the small amplitudes in this region. Figures 10a and b show an increase in period at x = -6500 km to 93 hours (3.87 days) and 90 hours (3.75 days), respectively, and a decrease at x = 6500 km to 39 hours (1.65 days) for a and b, respectively. Figure 8 shows only an increase at x = 6500 km to 100 hours (4.17 days) and 93 hours (3.87 days) for a and b, respectively. This abnormal behavior could be connected to the departure of the growth rate from the linear behavior illustrated in Fig. 5.

Figure 11 is an overview of the phase tilt for all three time segments. Although they are not the same, they are similar in the region from x = 3875 to x = -12000 km. They tend to be different in the region where the amplitude is small.

The envelope of the wave packet is evaluated at y = -750 km where the wave disturbance amplitude is large. The normalized ψ' field is used because the waves are still growing and results are something close to a sinusoidal variation. This envelope, $\langle\psi'(x)\rangle$, is obtained by recording the average of the magnitudes of the maximum and minimum $\psi'/|\psi|_{ave}$ values that occur at each longitude over a period of 7 days. Here, $|\psi|_{ave}$ is the root mean square ψ'. Figure 12 shows the wave packet of all three time segments for y = $\pm$ 750 km. Note that the maximum amplitude in Fig. 12 is near the point where the parallel flow growth rate drops to zero in Fig. 1.

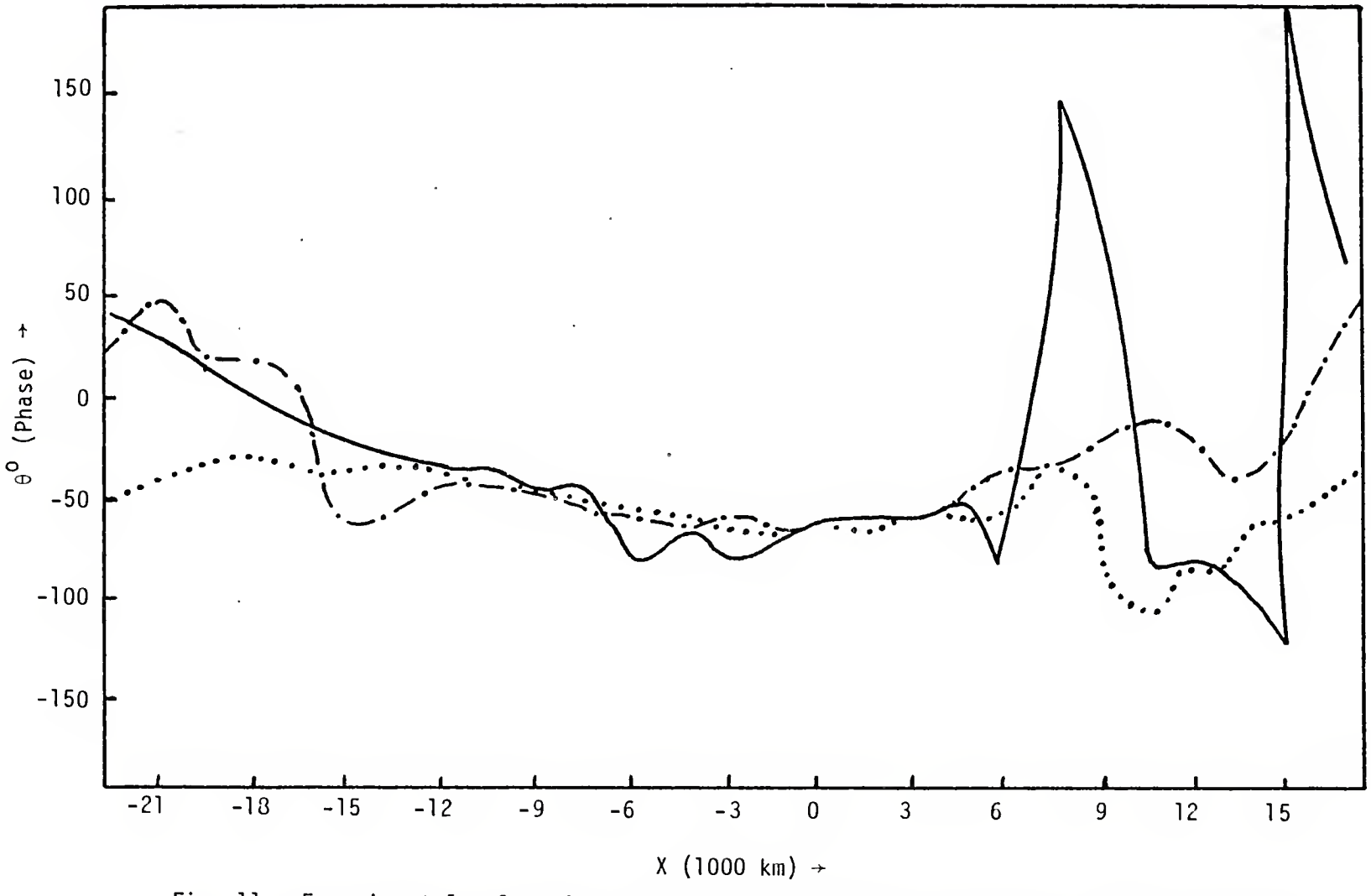

Fig. 11. Experiment I. Overview of phase tilt between y = 0 and y = ± 750 km for the time segments: (a) 80-87 days (...), (b) 125-133 days (·-·-) and (c) 150-157 days.

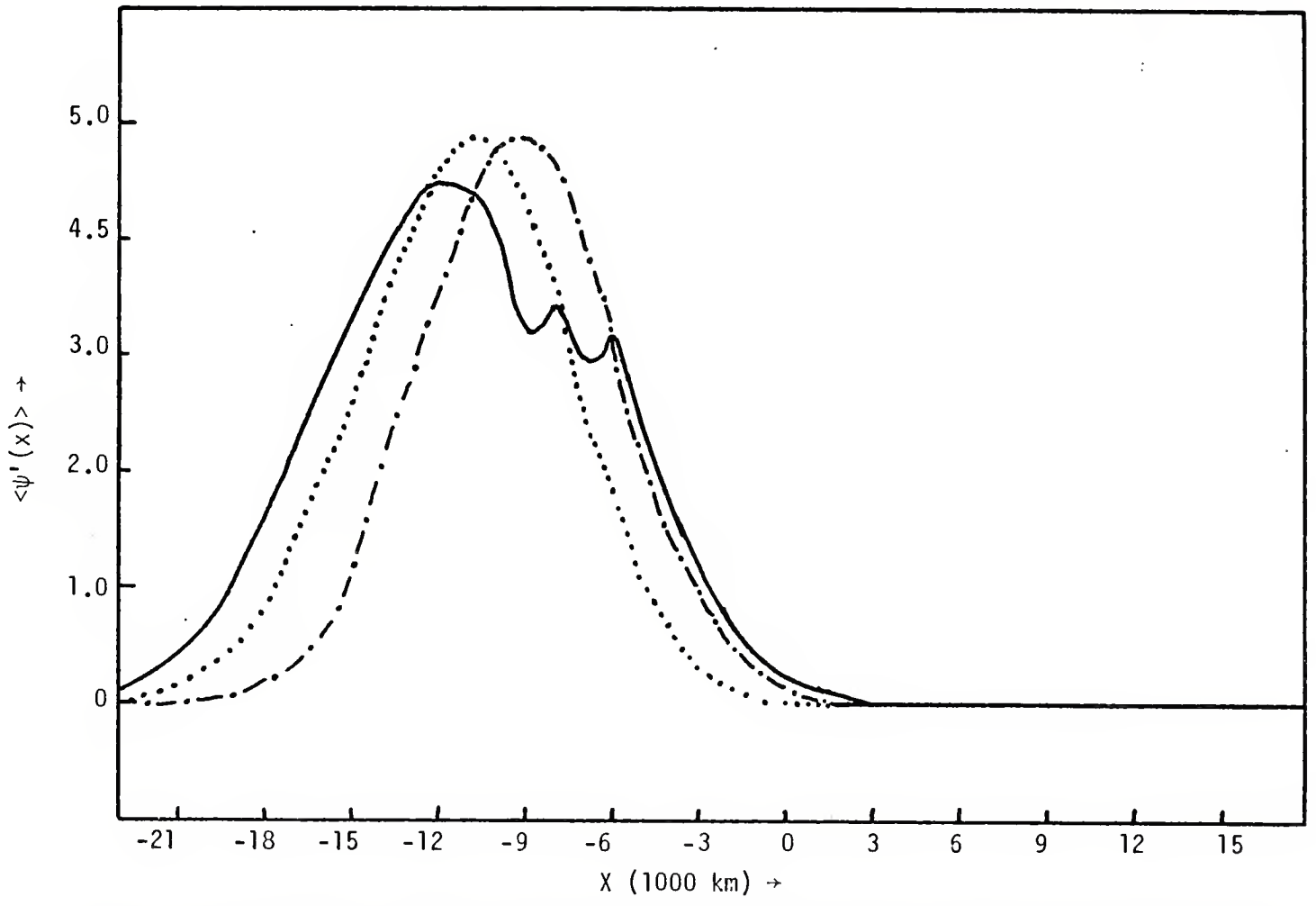

Fig. 12. Experiment I. Wave packet envelope, $\langle\psi'(x)\rangle$, of the numerical model for the time segments: (a) 80-87 days (...), (b) 125-133 days (·---·) and (c) 150-157 days (—).

Although they are not the same, it should be noted that they are downstream of the max jet core.

Tupaz et al. (1978) derived the disturbance kinetic energy equation to better understand the dynamics of barotropic instability. They found a number of energy terms but observed that the Reynolds stress term, $<(u'v' \partial\bar{u}/\partial y)>$, was the only dominate source for disturbance kinetic energy. This supported the large amplitudes and spatial gradients of ψ' encountered a considerable distance downstream of the jet. It is expected that this energy balance will also hold in this study. Since this is a region of tilt opposite to the shear, there is a conversion of mean flow kinetic energy to disturbance flow kinetic energy. Figures 1 and 2 illustrate the large energy conversion of this type for the parallel flow model.

Figures 13-16 show the phase angle θ of the wave disturbance as a function of y for three different time segments. The phase, θ_o, for the most unstable wavelength of the parallel flow model is also included (see Section 4). We note that the waves upstream of -10875 km tilt oppositely to the mean wind shear, which implies barotropic instability. In one case, the maximum tilt is downstream of x=0, which is where Tupaz et al. (1978) observed the maximum tilt. Between x = -10875 and x = 3750, the phase tilt compares closely to the parallel flow model θ_o. At the eastern boundary (Fig. 15b), θ_2^* compares rather well to θ_o, but θ_1^* and θ_3^* show excessive tilt for the comparatively weak instability in this region. This excessive fluctuation may partially be explained

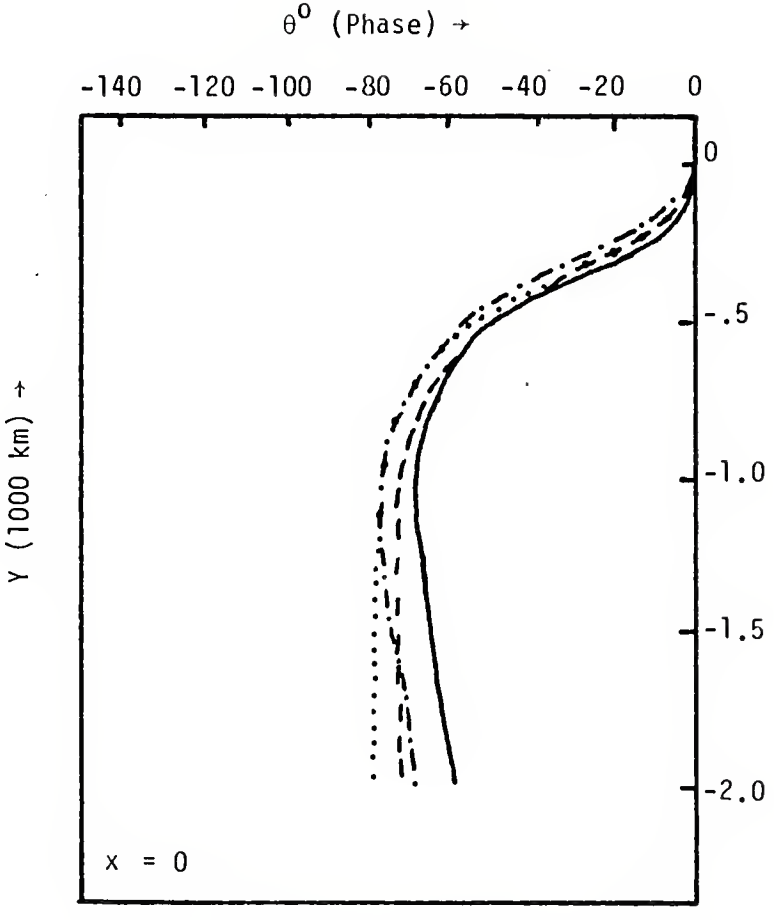

Figure 13. Experiment I. Comparison of phase θ of the numerical model for time segments (θ_1*) 80-87 days (...), (θ_2*) 125-133 days (.--.), (θ_3*) 150-157 days (—) and the most unstable wavelength of the parallel flow model, θ_o(---), for longitude x = 0.

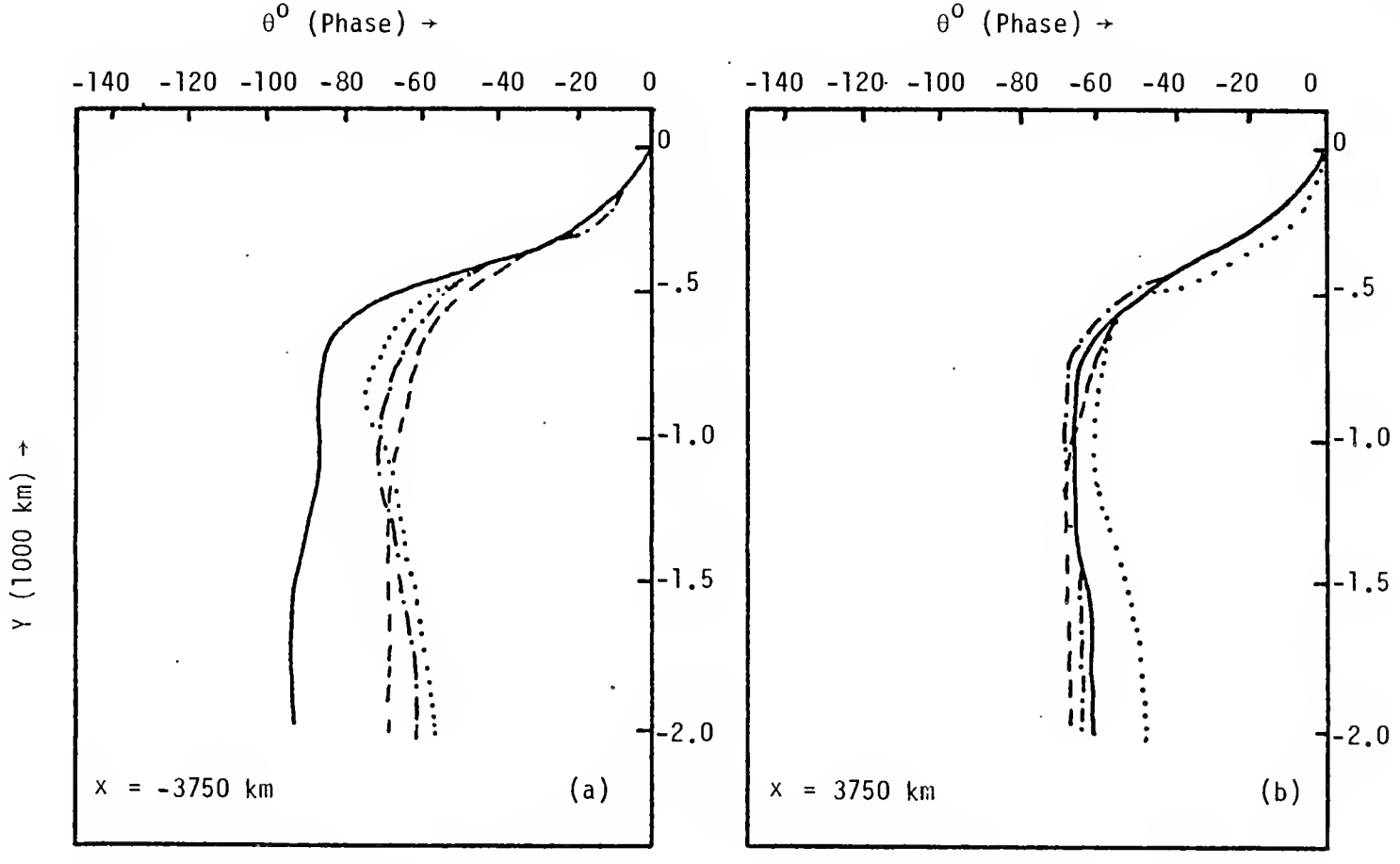

Fig. 14. Experiment I. Comparison of phase θ of the numerical model for the time segments (θ_1*) 80-87 days (...), (θ_2*) 125-133 days (.--.), (θ_3*) 150-157 days (—) and the most unstable wavelength of the parallel flow model, θ_o (---), for longitudes: (a) x = -3750 km and (b) x = 3750 km.

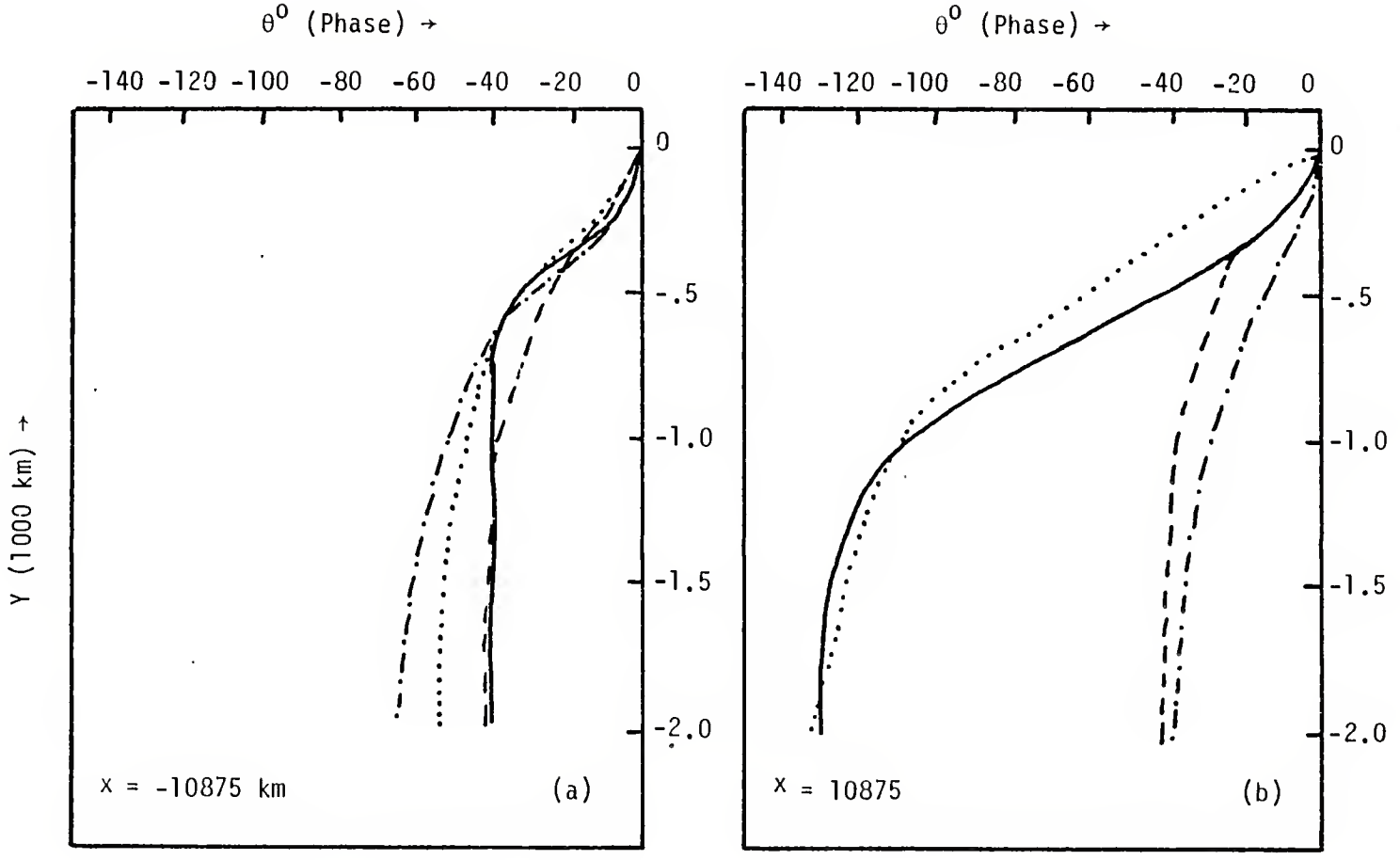

Fig. 15. Experiment I. Comparison of phase θ of the numerical model for time segments (θ_1*) 80-87 days (...), (θ_2*) 125-133 days (·-·-), (θ_3*) 150-157 days (—) and the most unstable wavelength of the parallel flow model, θ_o (---), for longitudes: (a) x = -10875 km and (b) x = 10875 km.

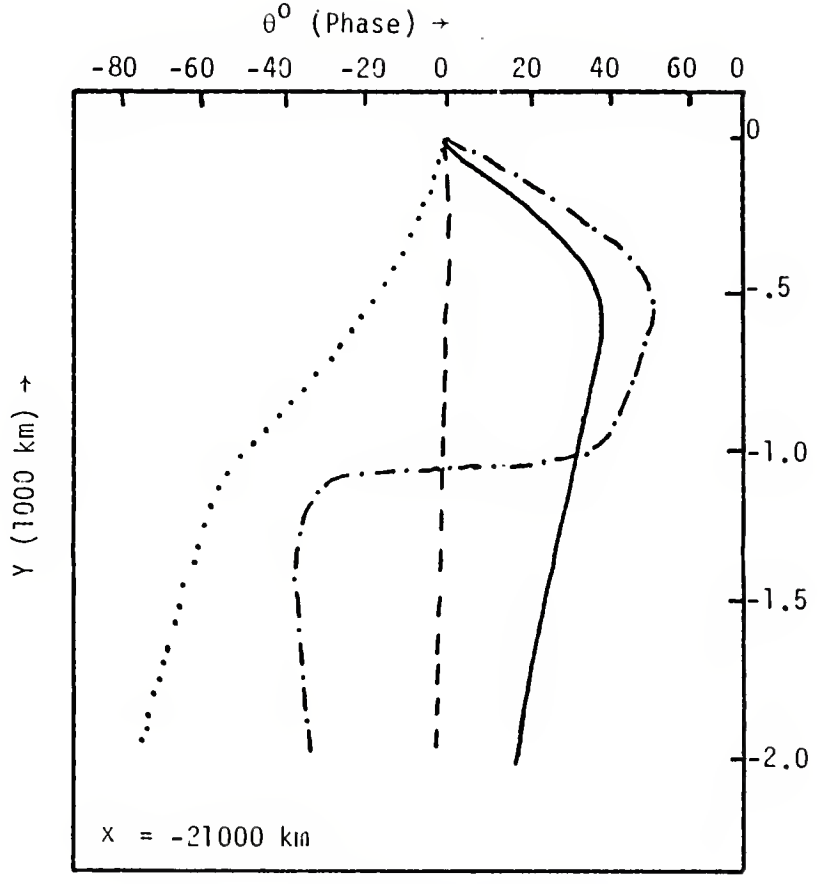

Fig. 16. Experiment I. Comparison of phase θ of the numerical model for time segments (θ_1*) 80-87 days (...), (θ_2*) 125-133 days (.-.-), (θ_3*) 150-157 days (——) and the most unstable wavelength of the parallel flow model, θ_o(---), for longitude X = -21000 km.

by the small amplitudes which are present in this region. Near the outflow boundary (Fig. 16) the tilt is reversed in θ_2^* and θ_3^*. This indicates dynamic stability or a flow of energy from the disturbance back to the mean flow. This can also be detected in Figs. 11b and c. In almost all cases, we observe that the tilt of the wave disturbance qualitatively adjusts to the local stability of the mean flow. Since the parallel flow model can only solve the most unstable discrete mode, dynamic damping is not indicated in Fig. 15 for the outflow region. Note that the phase tilt is unstable on the average. This is because the waves show a net growth on moving through the region.

The wavelengths for the numerical model are computed using the formula:

$$L = \frac{2\pi\ 2\Delta x}{\Delta\theta}\ , \qquad (5.3)$$

where $\Delta\theta$ represents the change in phase over $2\Delta x$. Equation (5.3) can be simplified and expressed in degrees resulting in

$$L = \frac{360^o\ 2\Delta x}{\Delta\theta^o}\ . \qquad (5.4)$$

In addition, a smoothing process is applied in those areas where the wavelength varies noticeably to give a more accurate picture of the wavelength throughout the channel. This calculation is made by choosing a questionable point (O) in the y domain of the phase field and adding 180^o to it. This

new phase is then located by moving in both x directions. The distance between the new phases is calculated in terms of the number of x grid points and multiplied by Δx to give the corrected, or smoothed, wavelengths. Figures 17-19 show the variation of wavelength, $L(x)^*$, for all three time segments at $y = \pm 750$ km. $L(x)_o$ represents the smoothed wavelength. Comparing the wavelengths of y=0 (not shown) and $y = \pm 750$ km, it is observed that the wavelengths are quite similar for each time period. The maximum wavelengths are within $\pm$ 4500 km of x=0 and tend to decrease toward the boundaries when the wavelength pattern becomes noisy. This is the same region that the phase tilt (Figs. 15b, 16) experiences large deviations from the parallel flow model due to the small amplitudes. Tupaz et al. (1978) observed that the wavelength at $y = \pm 750$ km was larger upstream and smaller downstream of x=0 than at y=0.

Figures 20-22 contain the spatial growth, m^*_{1-3}, computed from the numerical model, respectively. Figure 23 is the smoothed version of m^*_{1-3} and the spatial growth rate (m) of the parallel flow model obtained by using

$$m = -n/C_r \tag{5.4}$$

where C_r is the phase of the waves and n is the local growth rate (Tupaz et al., 1978). The value of m^*_{1-3} is computed directly from the wave packet envelope. In Fig. 22, we see that m^*_{1-3} has a larger maximum than m and the maximum is shifted slightly upstream from the jet maximum. All three

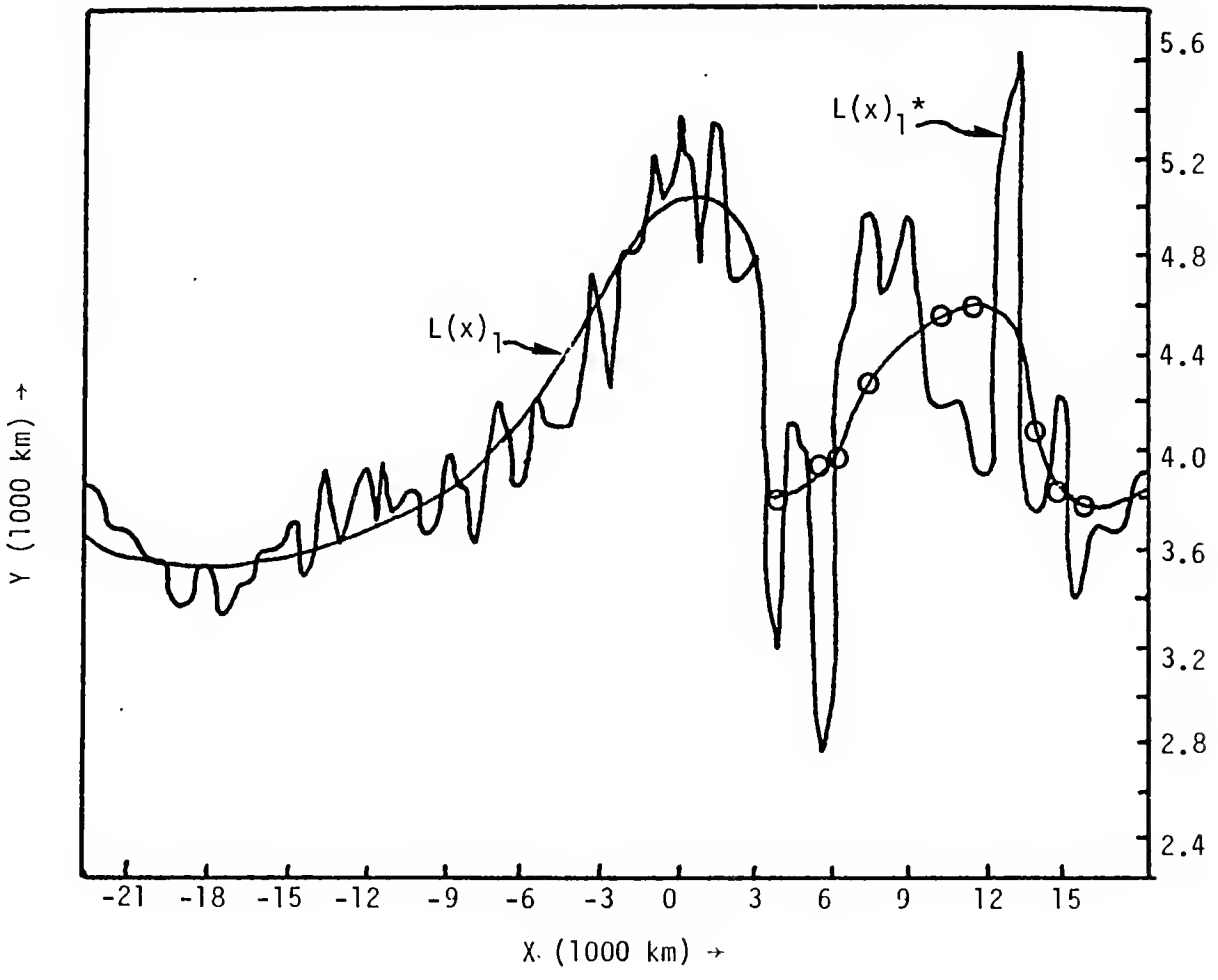

Fig. 17. Experiment I. Latitude y = ± 750 km. (a) Wavelength $L(x)_1$* for time segment 80-87 days. (b) Wavelength $L(x)_1$ computed by smoothing $L(x)_1$*.

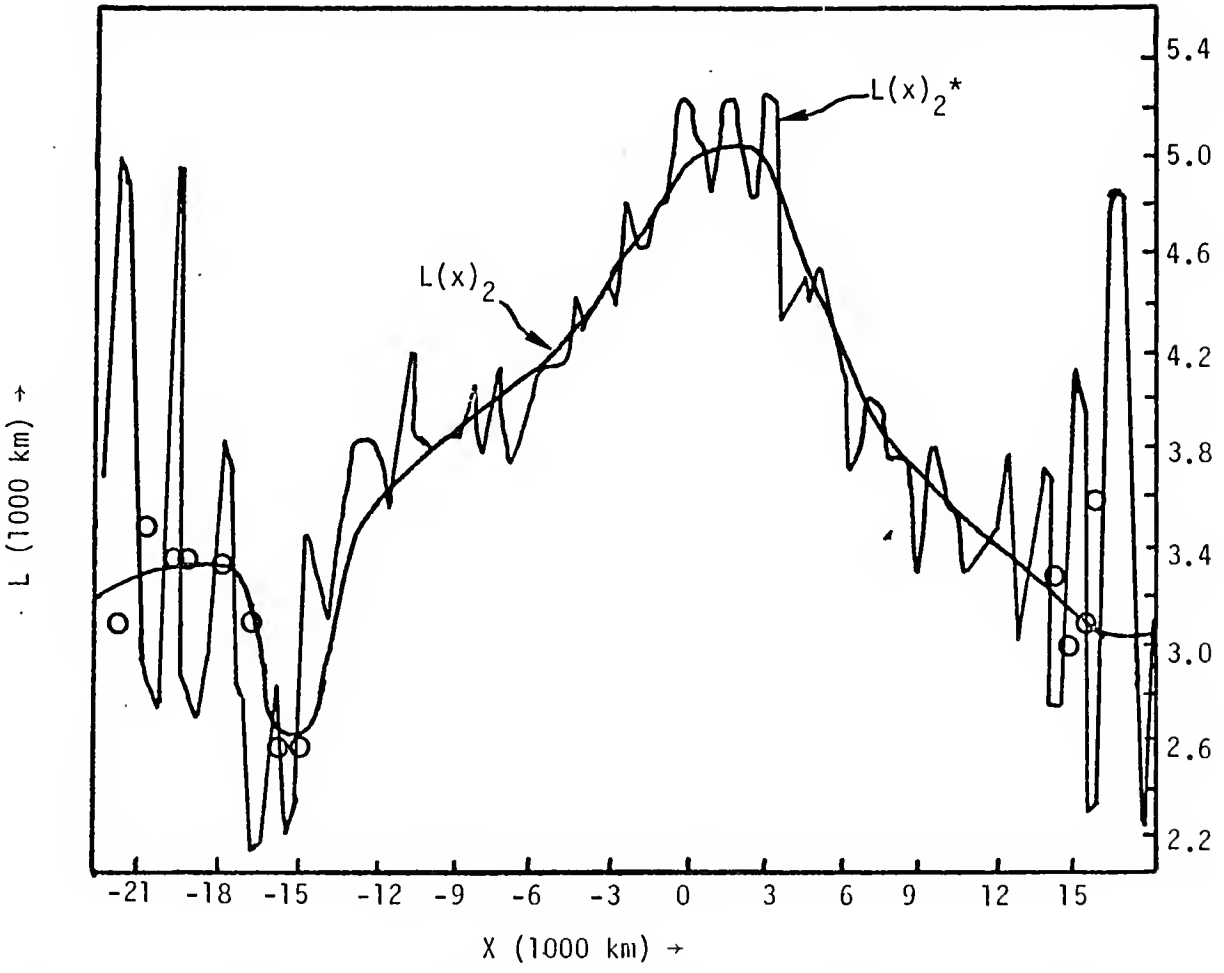

Fig. 18. Experiment I. Latitude y = ± 750 km (a) Wavelength $L(x)_2^*$ for time segment 125-133 days. (b) Wavelength $L(x)_2$ computed by smoothing $L(x)_2^*$.

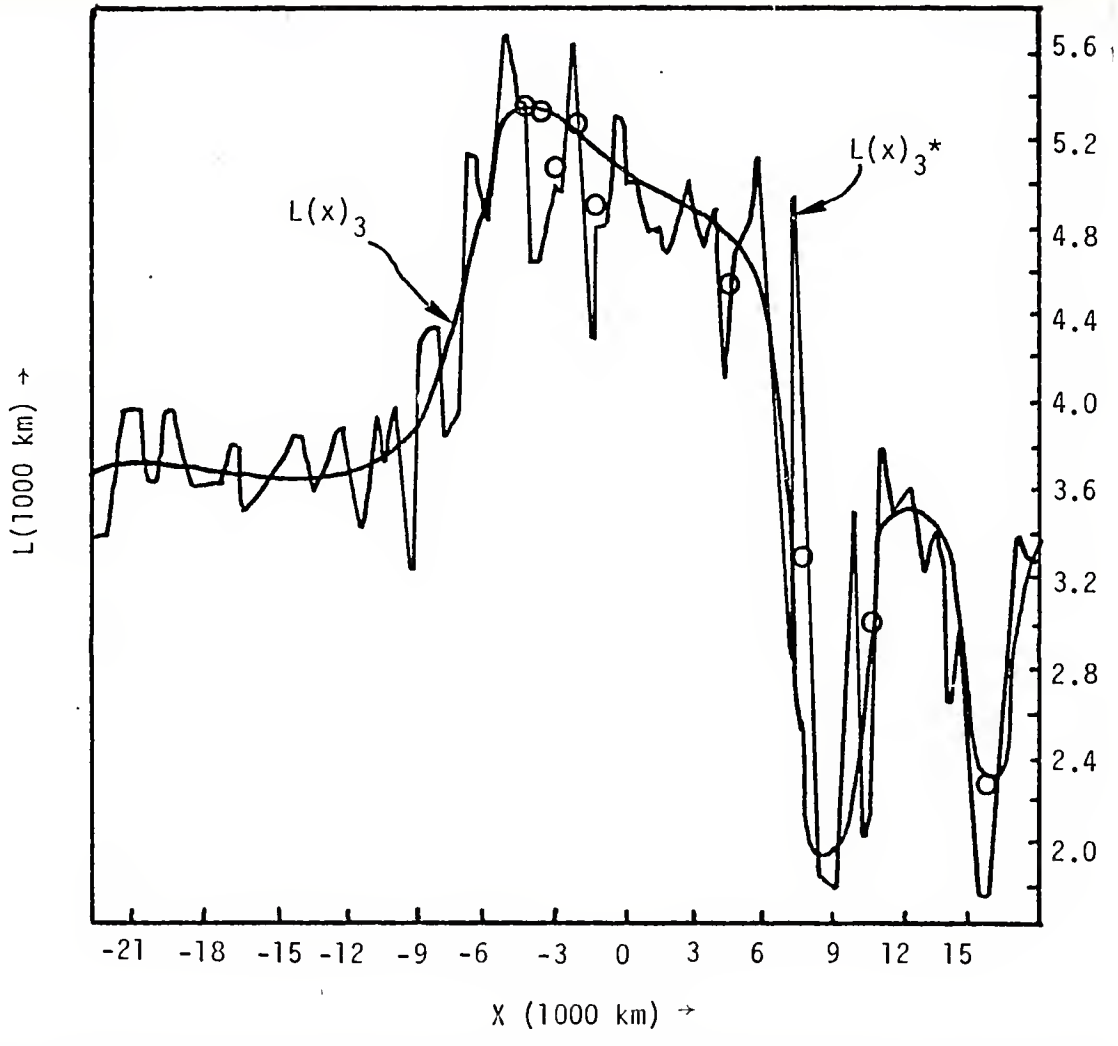

Fig. 19. Experiment I. Latitude y = ± 750 km. (a) Wavelength $L(x)_3$* for time segment 150-157 days. (b) Wavelength $L(x)_3$ computed by smoothing $L(x)_3$*.

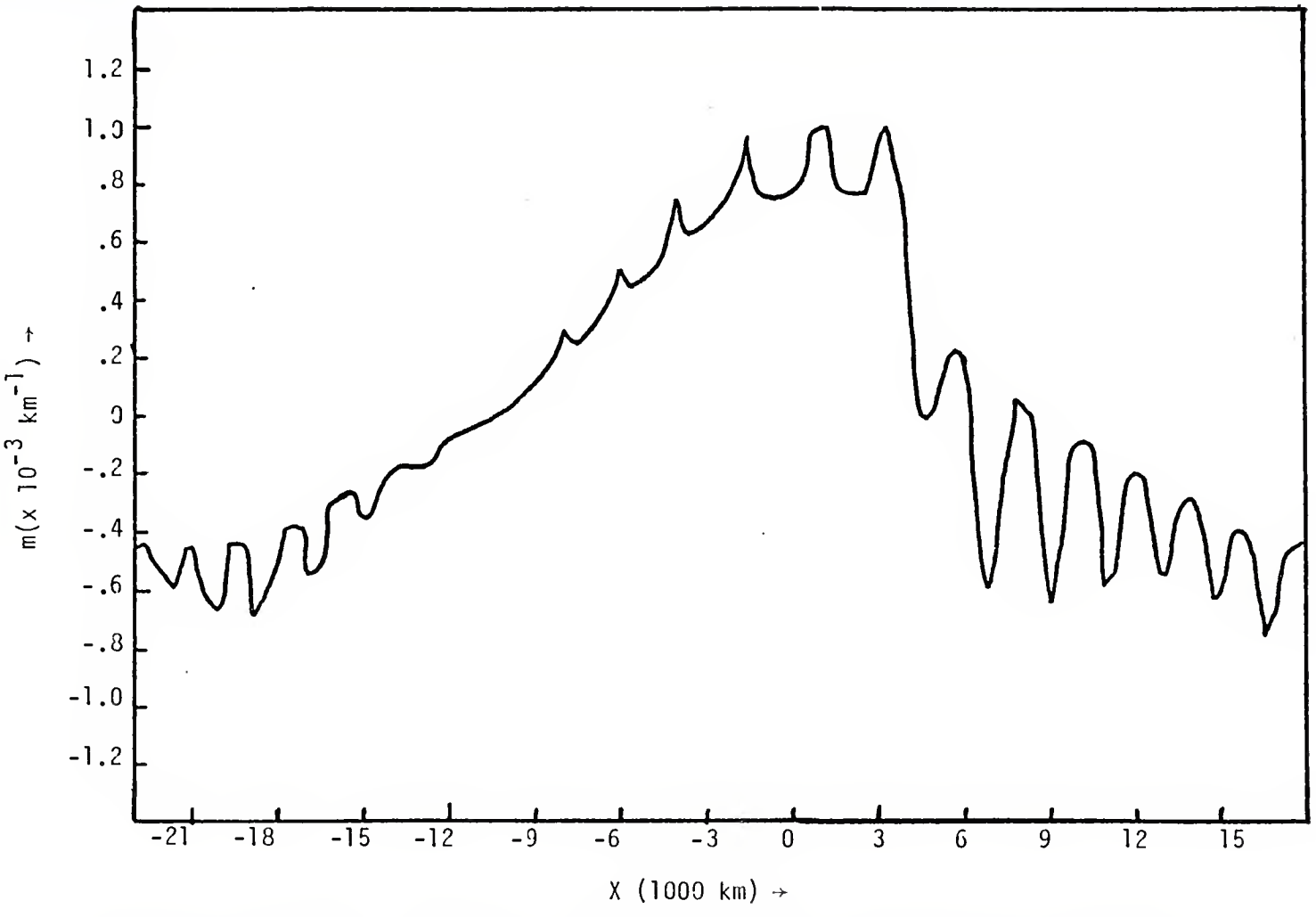

Fig. 20. Experiment I. Spatial growth rate, $m(x)_1$*, for time segment 80-87 days.

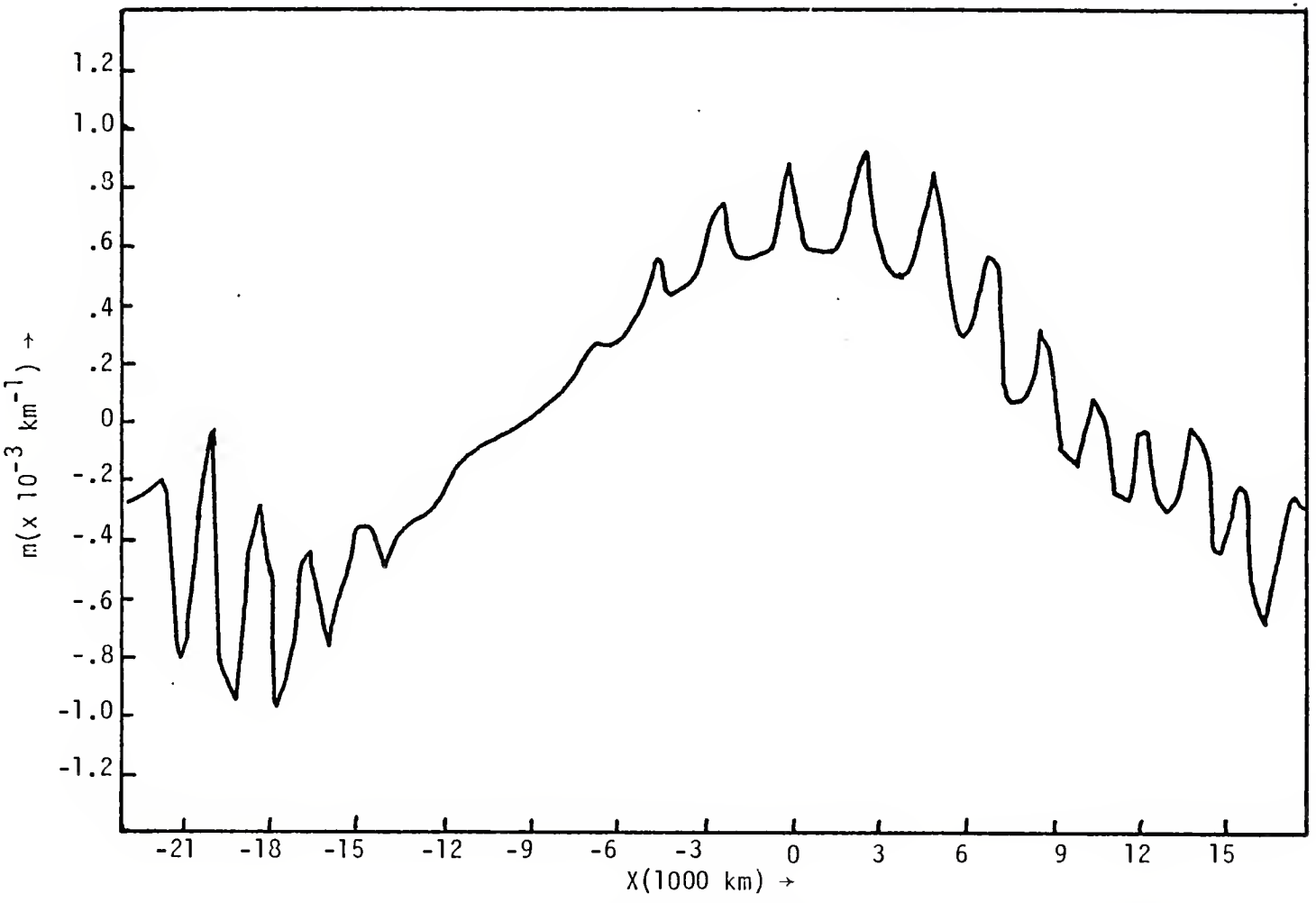

Fig. 21. Experiment I. Spatial growth rate, $m(x)_2$*, for time segment 125-133 days.

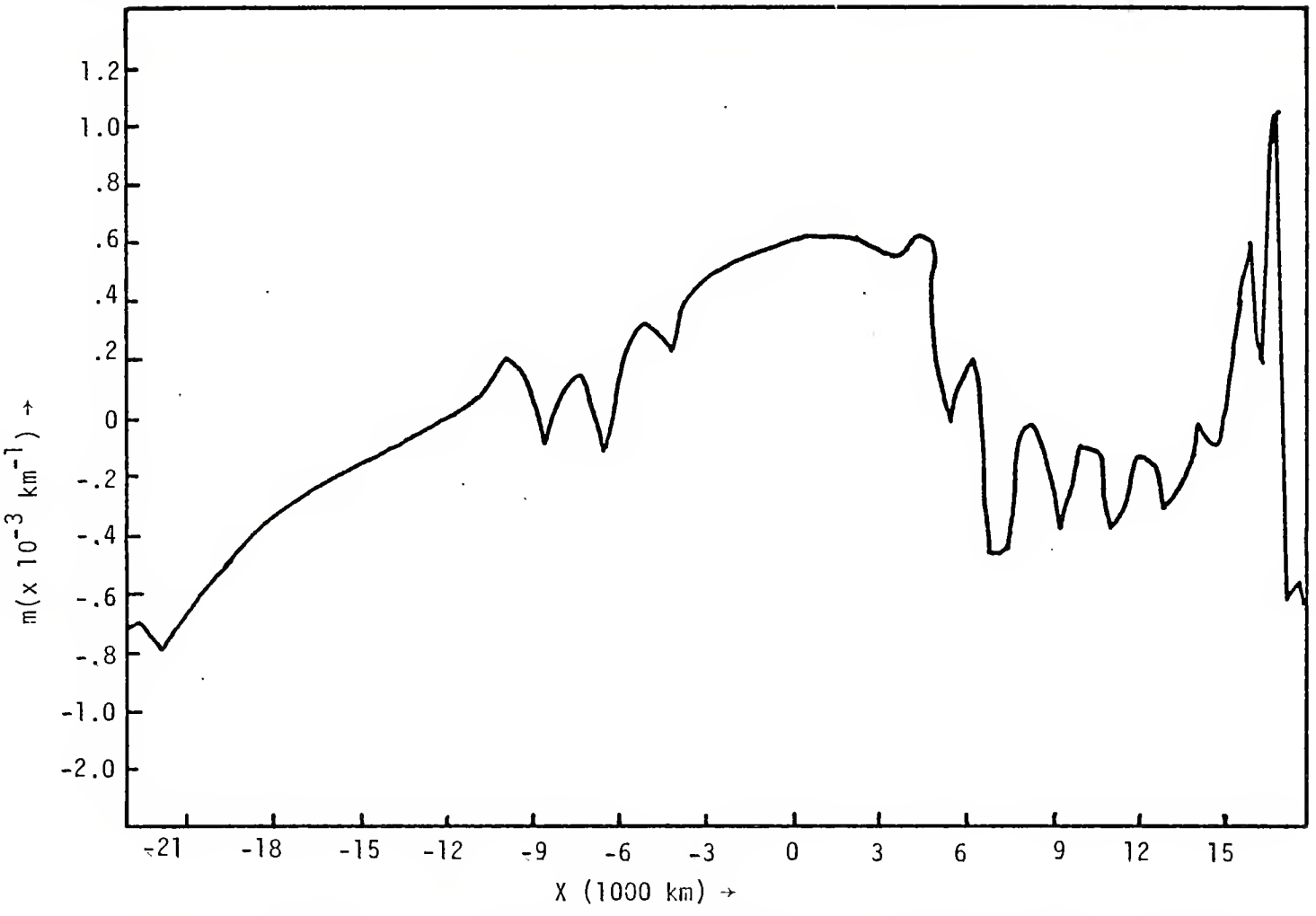

Fig. 22. Experiment I. Spatial growth rate, $m(x)_3^*$, for time segment 150-157 days.

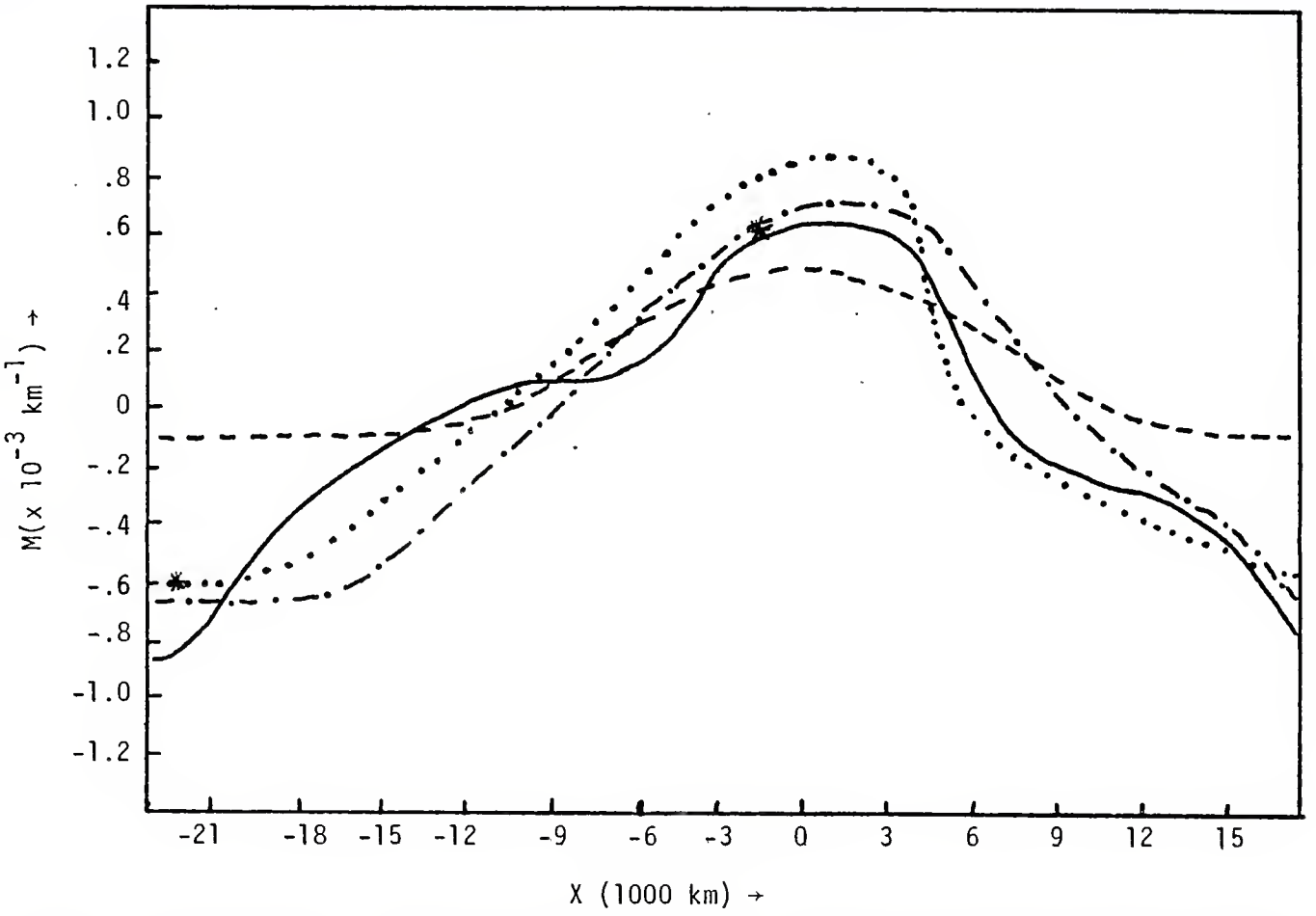

Fig. 23. Experiment I. Comparison of the spatial growth rates of the numerical model for time segments $(m(x)_1^*)$ 80-87 days (...), $(m(x)_2^*)$ 125-133 days (.-.-), $(m(x)_3^*)$ 150-157 days (—) and m(x) computed from the parallel flow model.

(*) represents the maximum and minimum observed by Tupaz et al. (1978).

curves pass through zero at the same point in which the wave packet envelopes are a maximum (see Fig. 12). Note again the noisy pattern near the eastern boundary. Tupaz et al. (1978) observed these same features except that the m^* curve was skewed to the left with respect to m and the jet maximum. This was the result of the tilt structure in the wave lagging spatially behind the expected value from the local stability conditions. The (*) represents the maximum and minimum observed by Tupaz et al. (1978). Note the similarity of the maximum and minimum to m_3^* and m_{1-2}^*, respectively. The reason that m_{1-3}^* shows more damping in the outflow region than the parallel flow model is because the latter can only give the eigensolutions of the most unstable mode.

VI. NUMERICAL RESULTS FOR EXPERIMENT II

Experiment II is the frictionless case and employs the same parameters and calculations procedures that are used in Experiment I. However, although the integration for this experiment is extended for 170 days, only the time segments of 80-87 days and 125-133 days are included in these results.

Figure 24 shows the root mean square ψ' for the entire domain. Note that the total growth is nine orders of magnitude greater than that observed in Experiment I (see Fig. 5). In addition, the curve in Fig. 24 is more linear in appearance than Fig. 5 but still experiences the departures from the linear behavior during the same time interval that were observed when friction was included.

The periods at y=0 and y = $\pm$ 750 km show very little variation and closely resembled those pictured in Figs. 7 and 8. The predominating period which is representative for the entire channel is the same as Experiment I (77 hours or 3.2 days).

Figure 25 is an overview of the phase tilt for the two time segments. The region of similarity extends from x = 5000 km to x = -15,000 km. When the amplitudes are small, the behavior becomes erratic as observed in Experiment I (see Fig. 11).

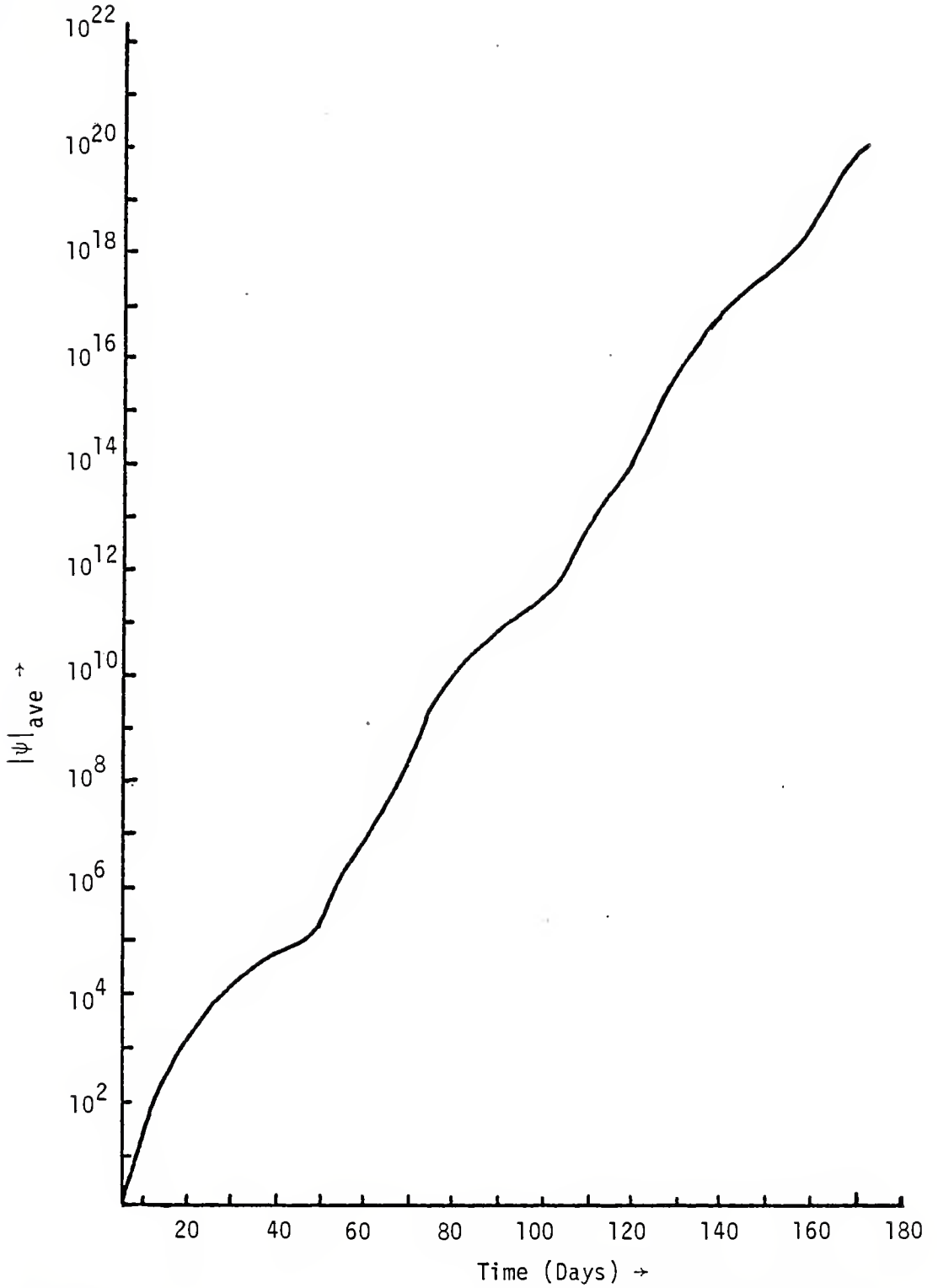

Fig. 24. Experiment II. $|\psi|_{ave}$ as a function of time, where $|\psi|_{ave}$ is the root mean square of ψ'.

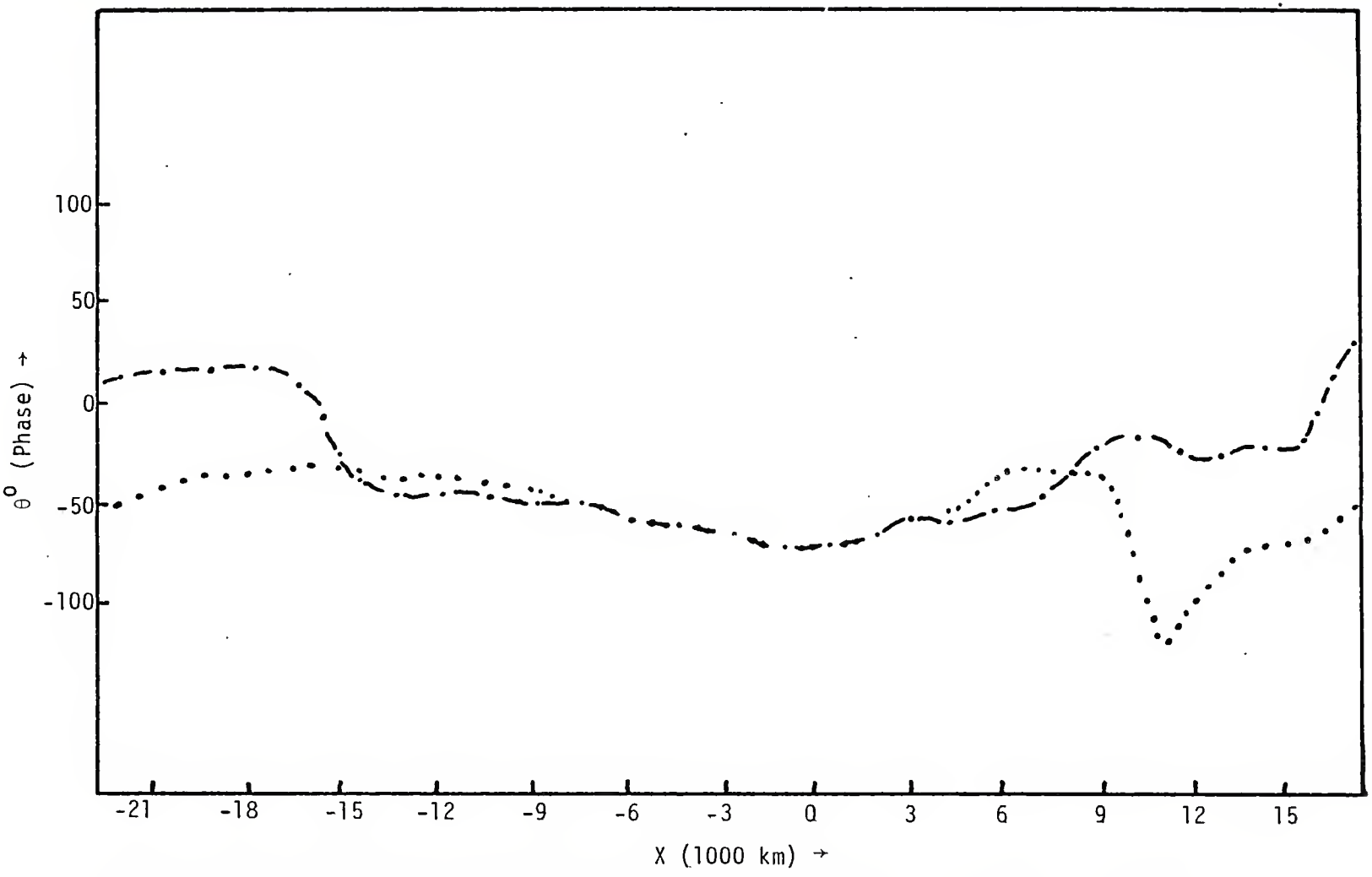

Fig. 25. Experiment II. Overview of the phase tilt between y = 0 and y = + 750 km for the time segments: (a) 80-87 days (...) and (b) 125-133 days (----).

The wave packet envelope, $\langle\psi'(x)\rangle$, is shown in Fig. 26. When comparing Fig. 26 to Fig. 12, it is observed that the curves are almost identical. Since the tilt is opposite to the shear, there is a conversion of mean flow kinetic energy to disturbance flow kinetic energy.

Figures 27-30 show the phase angle tilt of the wave disturbance y-structure compared to the most unstable wavelength of the parallel flow model θ_o. In both cases, the maximum tilt was at x=0. Comparing them to Figs. 13-16 in Experiment I, we see a similar structure except for Figs. 27 and 29a which show greater tilt between 500-750 km. Note again the excessive tilt of θ_1^* for the comparatively weak instability shown in Fig. 29b, and the elimination of the growth of θ_2^* of y greater than -1000 km in Fig. 30 for the Figs. 15b and 16, respectively, in Experiment I. The curve for θ_2^* stresses the dynamic stability which can also be observed in Fig. 25b.

The wavelength patterns for y=0 and y = $\pm$ 750 are very similar to those observed in Experiment I. The maximum wavelength occurred within $\pm$ 4000 km of x=0.

The spatial growth rates (Figs. 31-33) are near mirror images of Figs. 20, 21 and 23. The growth rates are a little larger than in Experiment I as would be expected because there is no friction.

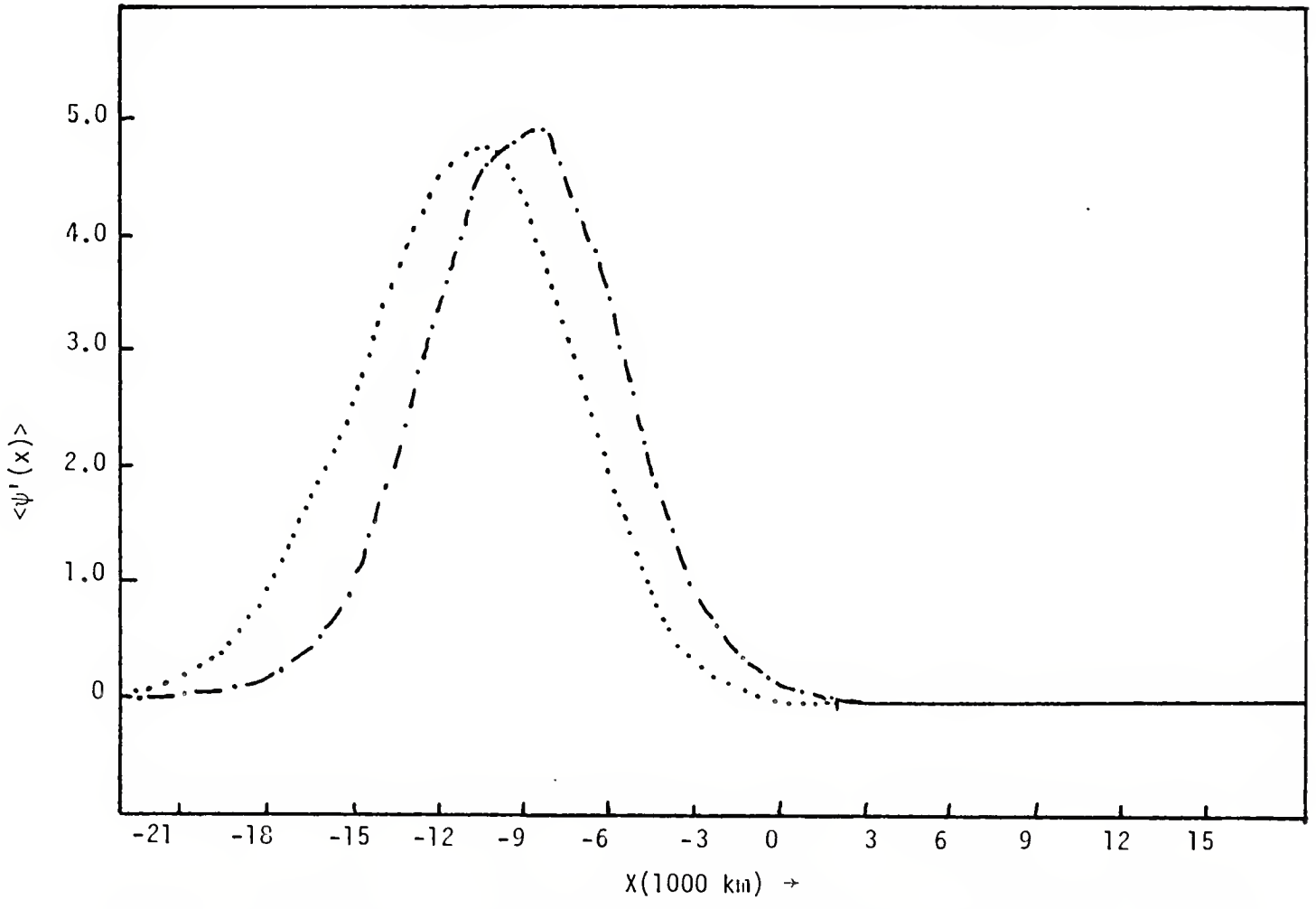

Fig. 26. Experiment II. Wave packet envelope, $\langle\psi'(x)\rangle$, of the numerical model for the time segments: (a) 80-87 days and (b) 125-133 days.

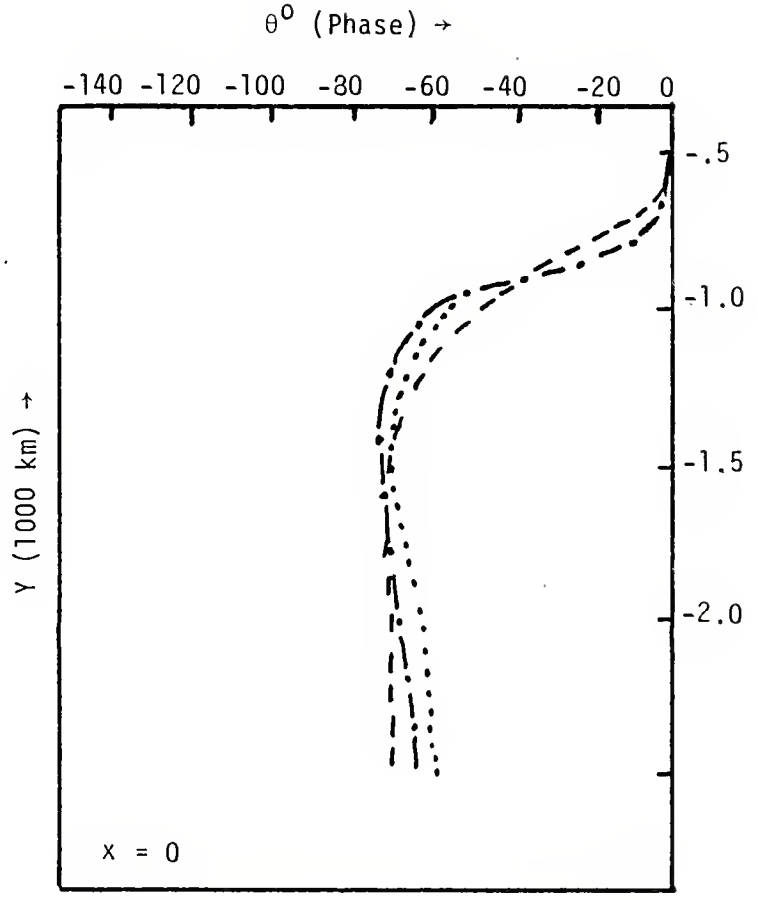

Fig. 27. Experiment II. Comparison of phase θ of the numerical model for time segments (θ_1*) 80-87 days(...), (θ_2*) 125-133 days (·-·-) and the most unstable wavelength of the parallel flow model, θ_o(---), for longitude X = 0.

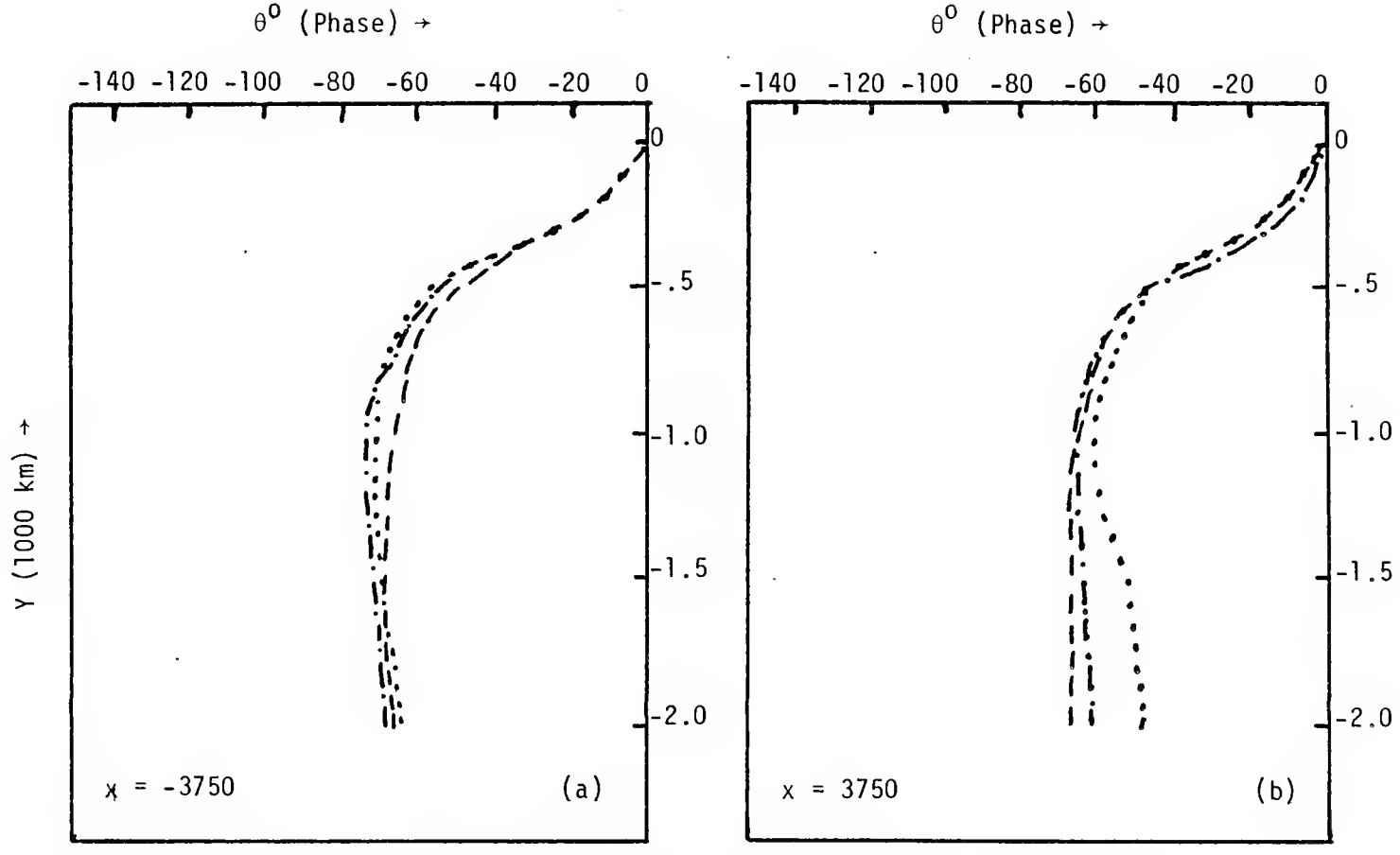

Fig. 28. Experiment II. Comparison of phase θ of the numerical model for time segments (θ_1^*) 80-87 days (...), (θ_2^*) 125-133 days (.---) and the most unstable wavelength of the parallel flow model, θ_o(---), for longitudes: (a) x = -3750 km and (b) x = 3750 km.

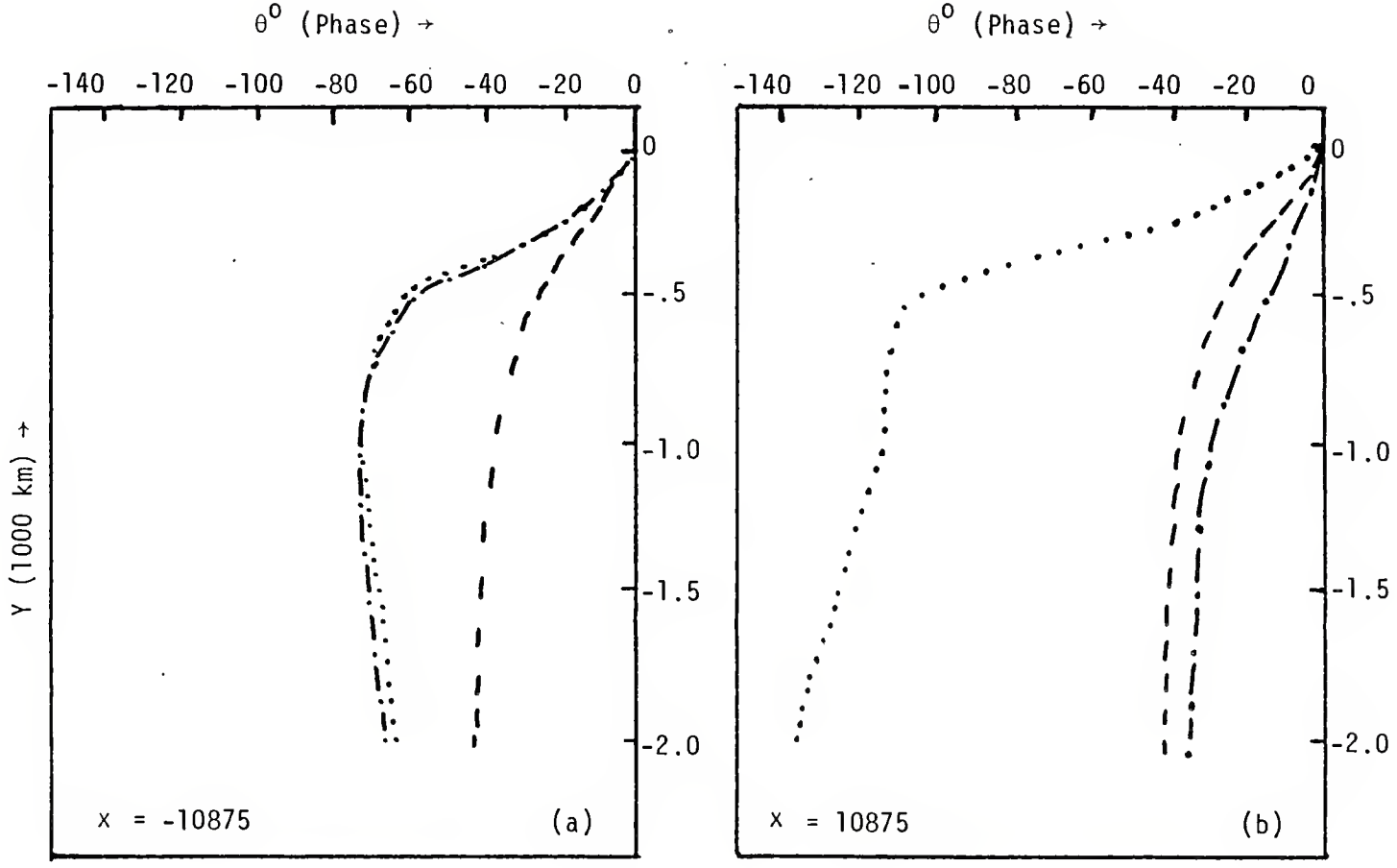

Fig. 29. Experiment II. Comparison of phase θ of the numerical model for time segments (θ_1*) 80-87 days (...), (θ_2*) 125-133 days (·-·-) and the most unstable wavelength of the parallel flow model, θ_o (---), for longitudes: (a) x = -10,875 km and (b) x = 10,875 km.

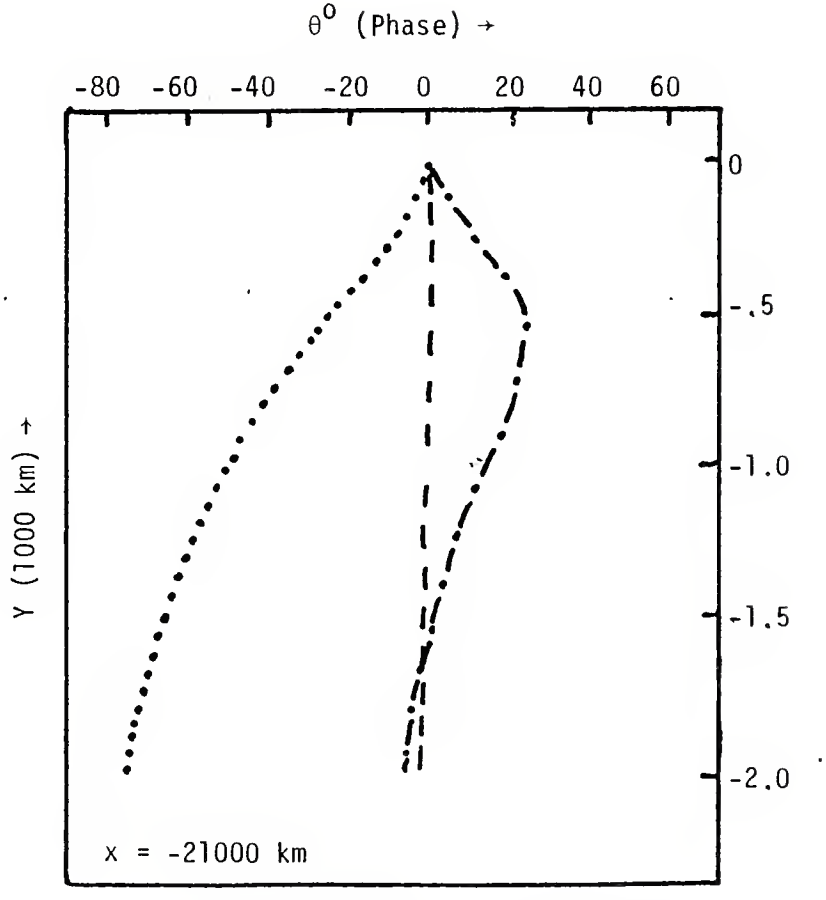

Fig. 30. Experiment II. Comparison of phase θ of the numerical model for time segments (θ_1*) 80-87 days (...), (θ_2*) 125-133 days (-·-) and the most unstable wavelength of the parallel flow model, θ_o(---), for longitude x = -21,000 km.

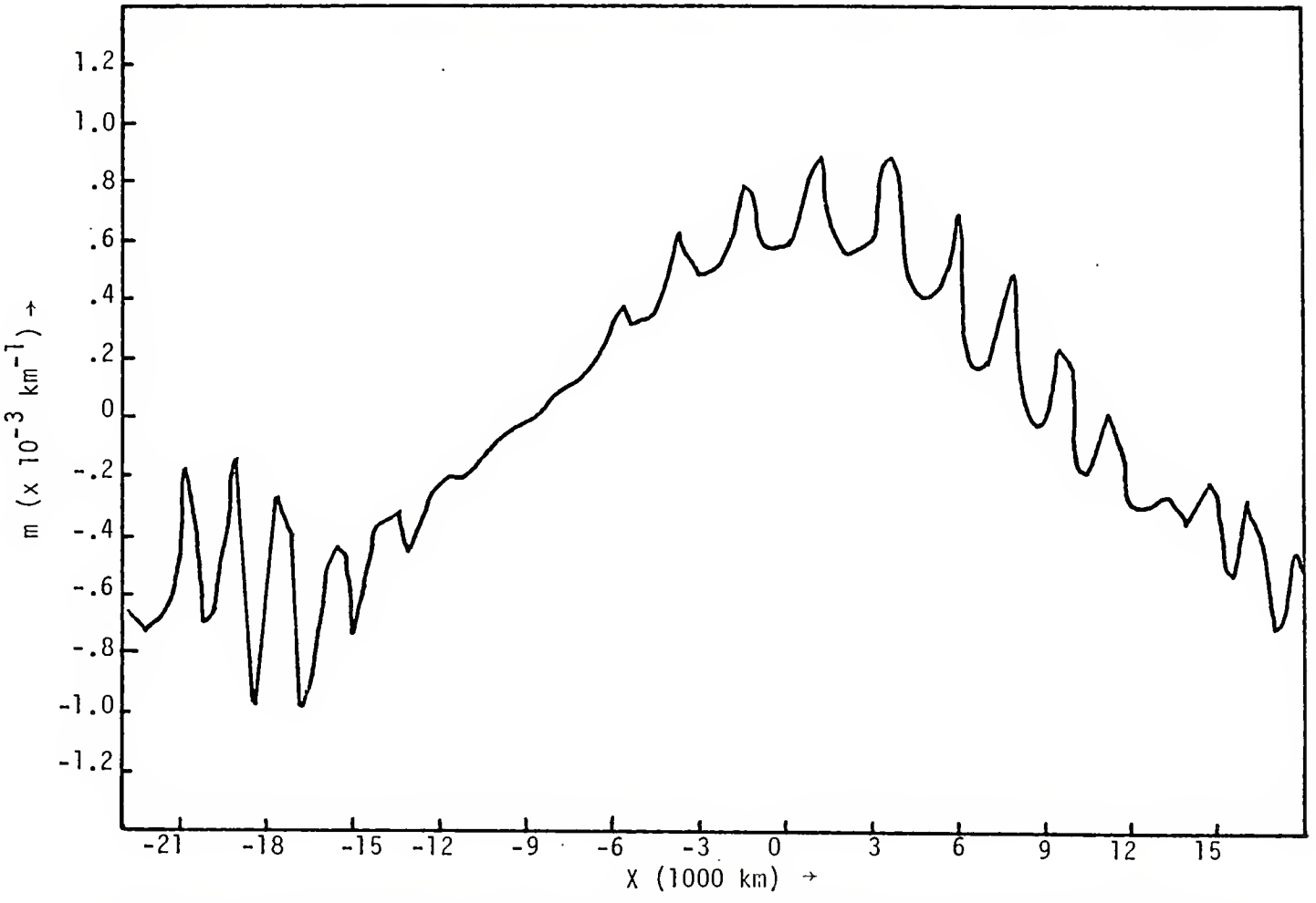

Fig. 31. Experiment II. Spatial growth rate, $m(x)_1$*, for time segment 80-87 days.

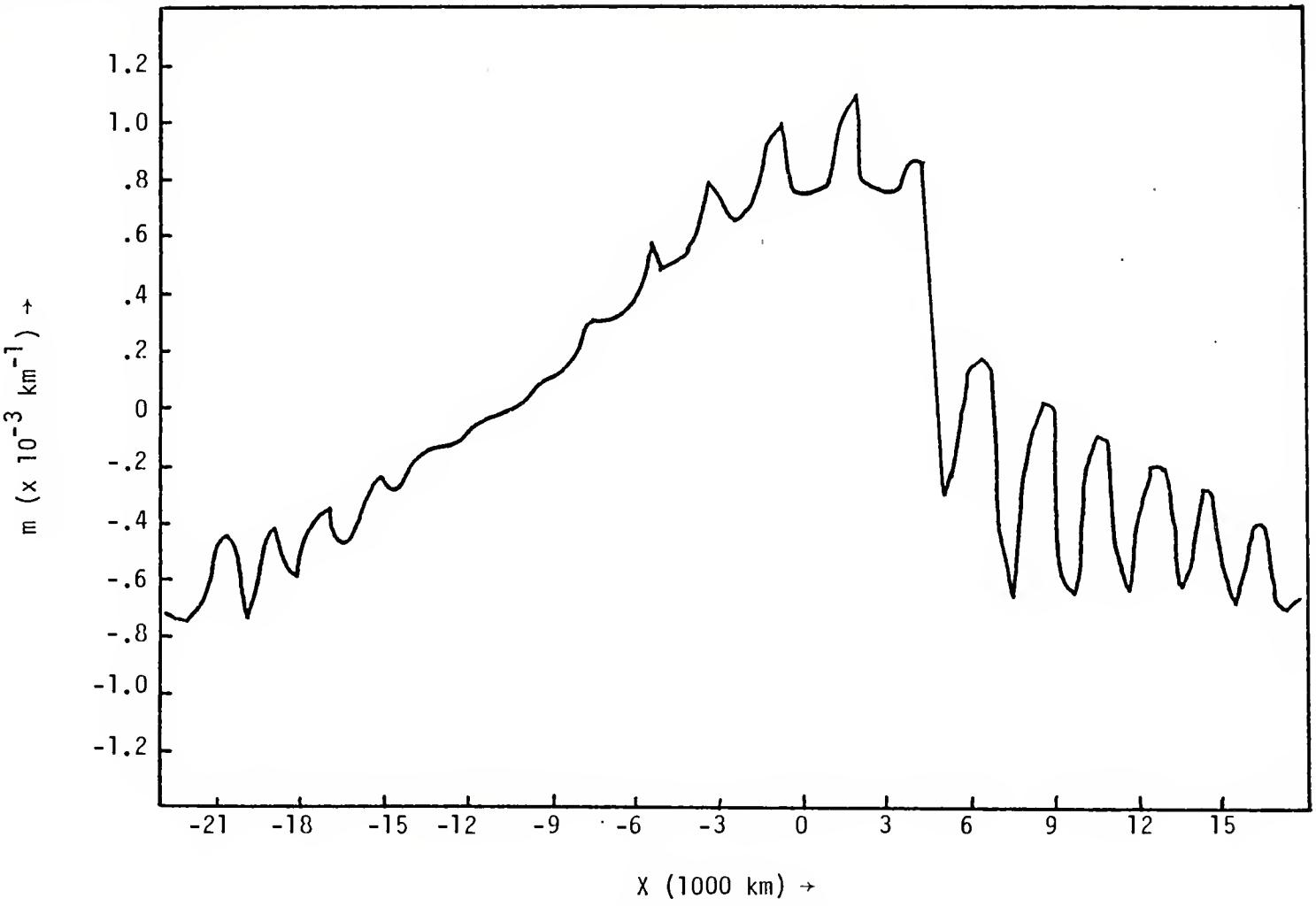

Fig. 32. Experiment II. Spatial growth rate, $m(x)_2^*$, for time segment 125-133 days.

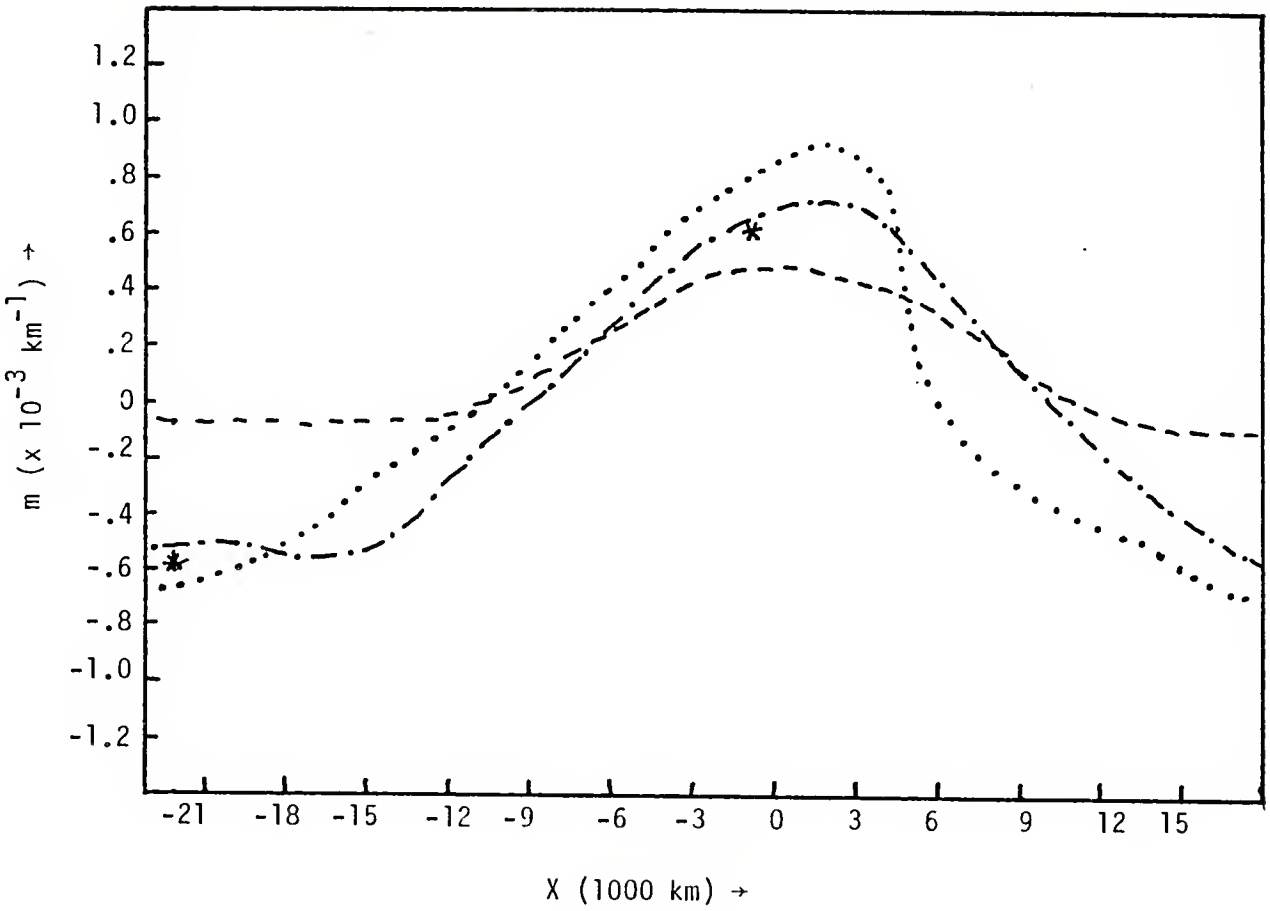

Fig. 33. Experiment II. Spatial growth rate, m(x) (---), from the parallel flow model and (a) $m(x)_1$* for 80-87 days (...) and (b) $m(x)_2$* for 125-133 days (·---) computed from numerical model.

(*) represents the maximum and minimum observed by Tupaz et al. (1978).

VII. SUMMARY AND CONCLUSIONS

This study solved the model developed by Tupaz et al. (1978) with different boundary conditions. They examined the behavior of linear waves in a zonally varying easterly jet which was barotropically unstable in certain longitudes. The waves were forced with a period ω on the eastern boundary and a radiation condition was applied on the western boundary to allow the waves to move smoothly out of the region. After a period of adjustment the solution at every point varied with period ω, but as each wave moved through the domain it experienced growth or decay in response to the local mean flow.

In the present study, the Tupaz model was modified by changing the boundary conditions to cyclic continuity on the eastern and western ends of the channel. In addition, the mean was modified slightly so that it satisfied cyclic continuity. Experiment I corresponded to Experiment I in Tupaz et al. (1978) and Experiment II was frictionless, but otherwise the same as Experiment I.

In Experiment I, the root mean square stream function grew with time because as each wave moved through the channel, its net growth was added when it reentered the region. This growth was approximately exponential with the departures from exponential growth having a period of about 36 days. In order to compare the wave behavior in this study with that of

Tupaz et al. (1978), the fields were normalized to remove the overgrowth in time. A procedure was developed to determine the phase and amplitude of the waves during a particular time segment. The following time segments were chosen for analysis: 80-87 days, 125-133 days, 150-157 days. The wave structure features were not the same for the three periods, but the features were very similar in the large amplitude regions. The predominant period was about 3.2 days which was very close to the forced period of 3.25 days used by Tupaz et al. (1978). The largest phase tilt was found near the jet maximum and in two of the segments the phase tilt reversed in the stable regions as was found by Tupaz et al. (1978). The amplitude of the wave envelope was a maximum near the point where the parallel flow growth rate was zero. The average of the maximum spatial growth rates was very close to the value obtained by Tupaz et al. (1978). This verified their result that the spatial variation in the growth rate could augment the maximum growth rate. The downstream wavelength was somewhat erratic, but it was generally a maximum near the jet maximum and it was a minimum where the jet was weak. The results for the frictionless case were similar, but the total growth was much larger.

In general, the wave behavior with cyclic boundary conditions was very similar to that obtained by Tupaz et al. (1978). However, the solutions in this thesis were more difficult to analyze because the wave structure in the three time segments was not the same. This was undoubtedly related to the non-exponential overall growths. Apparently as the

waves came out of the barotropic damping region and entered the jet region they did not have the structure to begin growth smoothly. In this region the wave phase structure was particularly erratic. When the present model was used to determine wave structure and behavior with other wind profiles, the structure should have been computed frequently and then the typical structure could have been obtained by averaging.

This study should be extended to the nonlinear case, by including a forcing term to maintain the mean flow when there are no waves present. When waves are introduced the modification of the mean flow could be studied.

BIBLIOGRAPHY

Arakawa, A., 1966: Computational Design for Long-Term Numerical Integrations of the Equations of Atmospheric Motion. Journal of Computational Physics, Vol. 1, 119-143.

Case, K. M., 1960: Stability of Plane Couette Flow. The Physics of Fluids, Vol. 3, 143-148.

Colton, D. E., 1973: Barotropic Scale Interactions in the Tropical Upper Troposphere during the Northern Summer. Journal of Atmospheric Sciences, Vol. 30, 1287-1302.

Haltiner, G. J., 1971: Numerical Weather Prediction, John Wiley & Sons, 317 pp.

Krishnamurti, T. N., 1971a: Observational Study of the Upper Tropospheric Motion Field during the Northern Hemisphere Summer. Journal of Applied Meteorology, Vol. 10, 1066-1096.

Krishnamurti, T. N., 1971b: Tropical East-West Circulations during the Northern Summer. Journal of Atmospheric Sciences, Vol. 28, 1342-1347.

Nitta, T., and M. Yanai, 1968: A Note on the Barotropic Instability of the Tropical Easterly Current. Journal of the Meteorological Society of Japan, Vol. 47, 127-130.

Pearson, R. A., 1974: Consistent Boundary Conditions for Numerical Models of Systems that Admit Dispersive Waves. Journal of Atmospheric Sciences, Vol. 31, 1481-1489.

Pedlosky, J., 1964: An Initial Value Problem in the Theory of Baroclinic Instability. Tellus, Vol. 16, 12-17.

Swarztrauber, P. and R. Sweet, 1978: Subroutine POISS, NCAR Computing Facility, Boulder, 5 pp.

Tupaz, J. B., R. T. Williams, and C.-P. Chang, 1978: A Numerical Study of Barotropic Instability in a Zonally Varying Easterly Jet. Journal of Atmospheric Sciences, Vol. 35, 1265-1280.

Williams, R. T., T. K. Schminke, and R. L. Newman, 1971: Effect of Surface Friction on the Structure of Barotropically Unstable Tropical Disturbances. Monthly Weather Review, Vol. 99, 778-785.

INITIAL DISTRIBUTION LIST

		No. Copies
1.	Defense Documentation Center Cameron Station Alexandria, Virginia 22314	2
2.	Library, Code 0142 Naval Postgraduate School Monterey, California 93940	2
3.	Professor C.-P. Chang, Code 63Cj Department of Meteorology Naval Postgraduate School Monterey, California 93940	2
4.	Professor R. T. Williams, Code 63Wu Department of Meteorology Naval Postgraduate School Monterey, California 93940	8
5.	Captain B. M. Nagle Air Weather Service Hq/DOA Scott AFB, Illinois 62225	5
6.	CDR J. B. Tupaz Code 3250 Pacific Missile Test Center Pt. Mugu, California 93042	2
7.	AFIT-CIP Wright-Patterson AFB, Ohio 45433	2
8.	Professor G. J. Haltiner, Code 63Ha Chairman, Department of Meteorology Naval Postgraduate School Monterey, California 93940	1
9.	Professor R. L. Elsberry, Code 63Es Department of Meteorology Naval Postgraduate School Monterey, California 93940	1
10.	Professor R. L. Haney, Code 63Hy Department of Meteorology Naval Postgraduate School Monterey, California 93940	1

11. Commanding Officer 1
Naval Environmental Prediction
Research Facility
Monterey, California 93940

12. Dr. A.Weinstein 1
Naval Environmental Prediction
Research Facility
Monterey, California 93940

13. Dr. T. Rosmond 1
Naval Environmental Prediction
Research Facility
Monterey, California 93940

14. Commanding Officer 1
Fleet Numerical Weather Central
Monterey, California 93940

15. Naval Oceanographic Office 1
Library, Code 3330
Washington, D. C. 20373

16. Meteorology Library, Code 63 1
Naval Postgraduate School
Monterey, California 93940

17. Director, Naval Research Laboratory 1
ATTN: Technical Services Information Center
Washington, D. C. 20390

18. Department of Oceanography, Code 68 1
Naval Postgraduate School
Monterey, California 93940

19. Office of Naval Research 1
Department of the Navy
Washington, D. C. 20360

20. Director 1
Naval Oceanography and Meteorology
National Space Technology Laboratories
Bay St. Louis, Mississippi 39520

21. Dr. A. Arakawa 1
Department of Meteorology
University of California
Los Angeles, California 90024

22. Dr. F. P. Bretherton 1
National Center for Atmospheric Research
P. O. Box 3000
Boulder, Colorado 80303

23. Professor J. G. Charney 1
54-1424
Massachusetts Institute of Technology
Cambridge, Massachusetts 02139

24. Dr. J. Holton 1
Department of Atmospheric Sciences
University of Washington
Seattle, Washington 98105

25. Dr. B. J. Hoskins 1
Department of Geophysics
University of Reading
Reading, United Kingdom

26. Professor T. N. Krishnamurti 1
Department of Meteorolgoy
Florida State University
Tallahassee, Florida 32306

27. Dr. E. N. Lorenz 1
Department of Meteorology
Massachusetts Institute of Technology
Cambridge, Massachusetts 02139

28. Dr. J. D. Mahlman 1
Geophysical Fluid Dynamics Laboratory
Princeton University
Princeton, New Jersey 08540

29. Professor N. A. Phillips 1
National Meteorological Center/NOAA
World Weather Building
Washington, D. C. 20233

30. Professor J. Pedlosky 1
Department of Geophysical Sciences
University of Chicago
Chicago, Illinois 60637

31. Professor A. L. Schoenstadt, Code 53Zh 1
Naval Postgraduate School
Monterey, California 93940

32. Professor Peter Webster 1
Department of Atmospheric Sciences
University of Washington
Seattle, Washington 98195

33. Dr. J. Young 1
Department of Meteorology
University of Wisconsin
Madison, Wisconsin 53706

Thesis 278762
N2323 Nagle
c.1 A numerical study of barotropic instability of a zonally varying jet with cyclic boundary conditions.